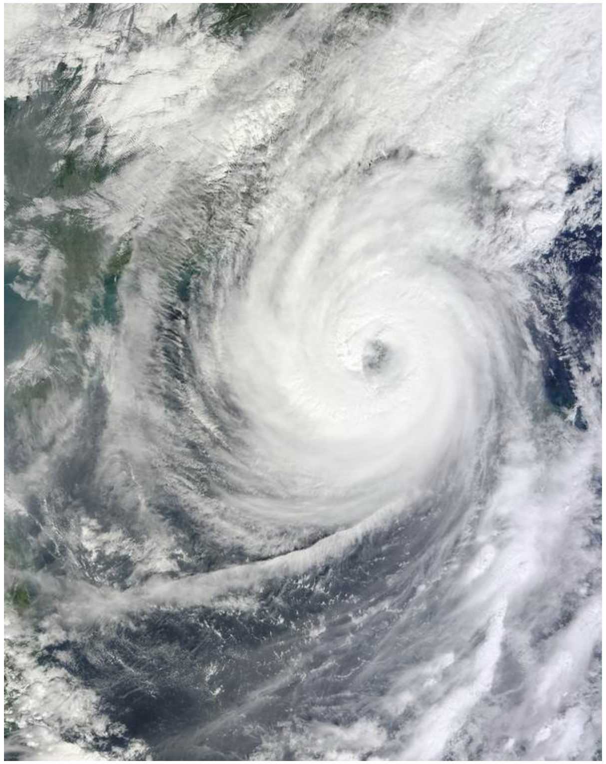

Yu. I. Troitskaya,
V.Kazakov,
N.Bogatov,
O.Ermakova,
M.Salin,
D.Sergeev
A. Kandaurov,
G.Baidakov
M.Vdovin

Institute of Applied Physics

Satellite remote sensing of severe weather conditions over the sea. II. On problems of scatterometry.

Tropical cyclones at SAR images

ASAR ENVISAT

The full-sized ASAR Wide Swath Mode image of Hurricane Rita, showing distinctive swirling patterns scoured into the sea surface by the storm's winds.

http://www.esa.int/spaceinimages/Images/2005/09/Rita_seen_in_full

Tropical cyclones at SAR images

ASAR ENVISAT

This close up detail from the ASAR Wide Swath Mode image of the area of the sea surface associated with Hurricane Katrina's eye shows a darker, smoother sea surface, due to the lack of winds at the central extreme low pressure.

http://www.esa.int/spaceinimages/Images/2005/08/Detail_of_Katrina_s_eye_seen_by_Envisat

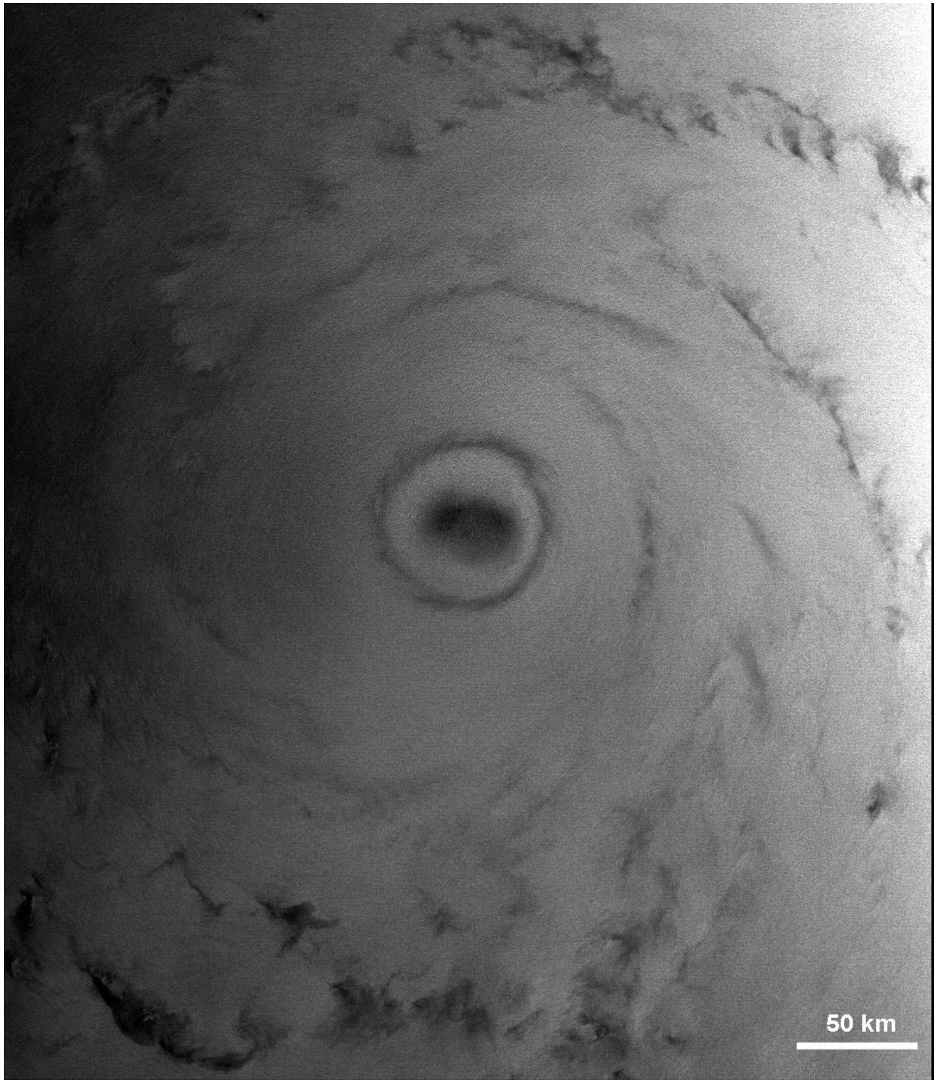

Tropical cyclones at SAR images

ASAR ENVISAT

This image shows the recent hurricane Isidore passing over the Gulf of Mexico and demonstrates how features related to all of the principal dynamics can be observed.
Radar Mode: WS
Orbit Direction: Descending
Radar Polarisation: VV

http://www.esa.int/spaceinimages/Images/2002/12/Hurricane_Isidore_ASAR_MERIS_-_21_September_2002

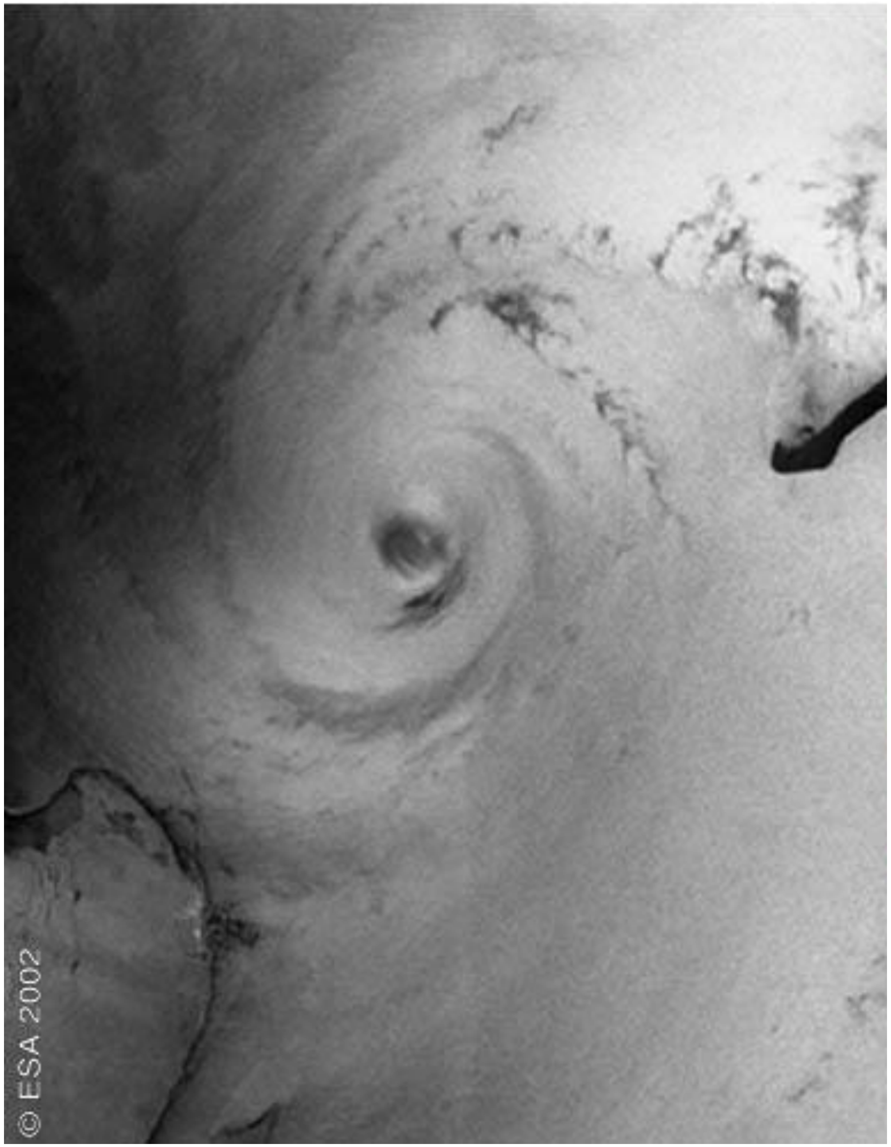

Tropical cyclones at SAR images

ASAR ENVISAT

Typhoon Megi
17 October
2010
01:22 UTC
VV

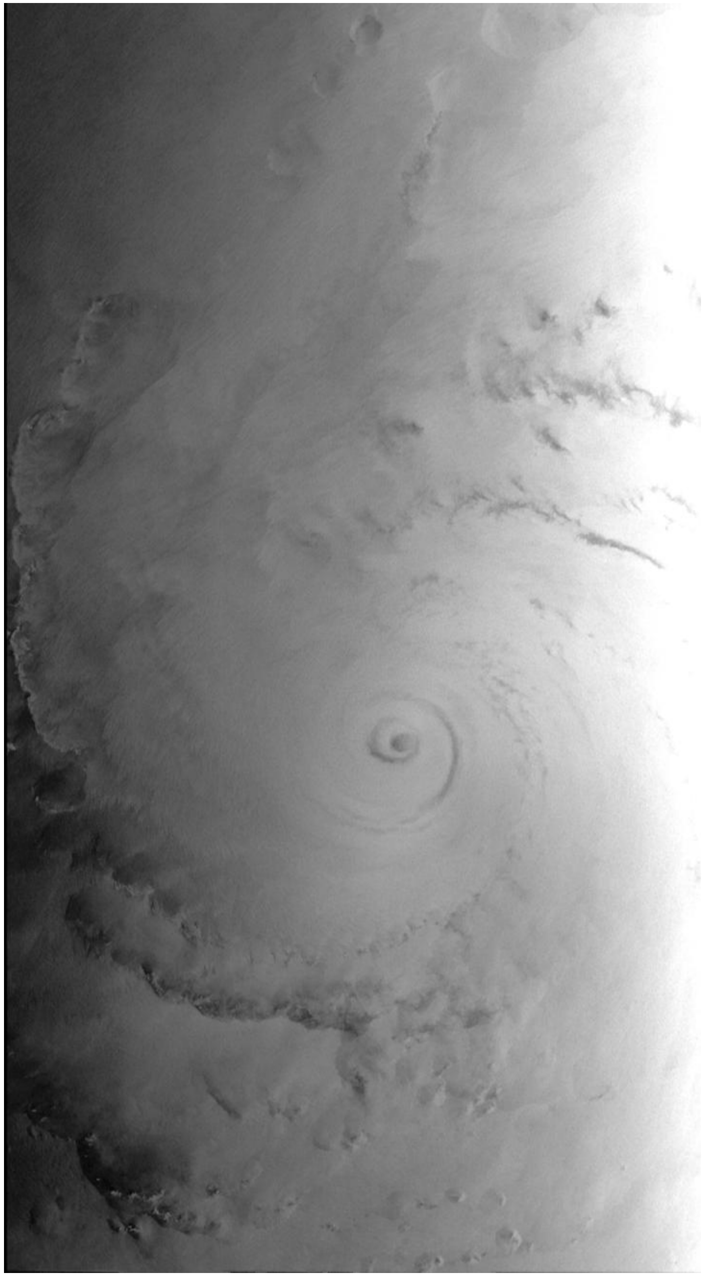

Tropical cyclones at SAR images

ASAR ENVISAT

Typhoon Aere

Envisat ASAR image with HH-polarization for 25 August 2004 at 01:52 UTC.

www.isprs.org/proceedings/2005/*.../376.pdf*

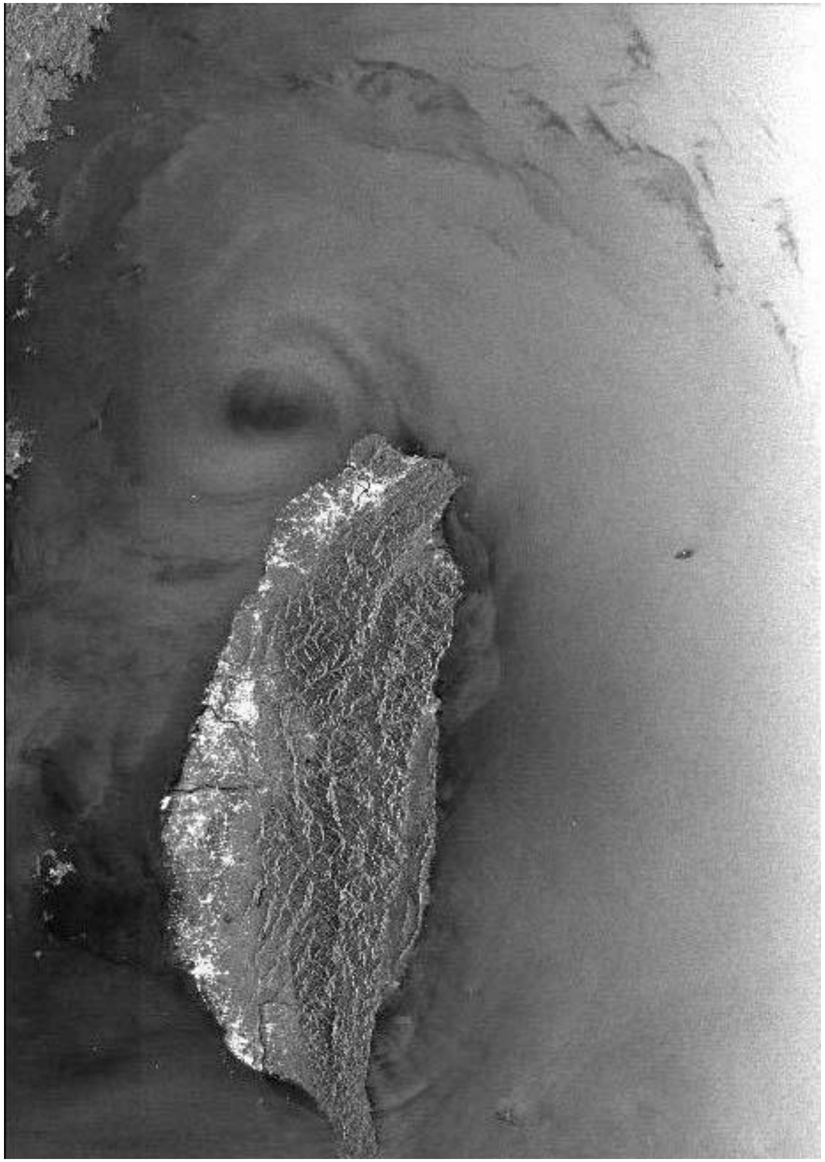

Tropical cyclones at SAR images

TerraSAR-X

Typhoon Megi

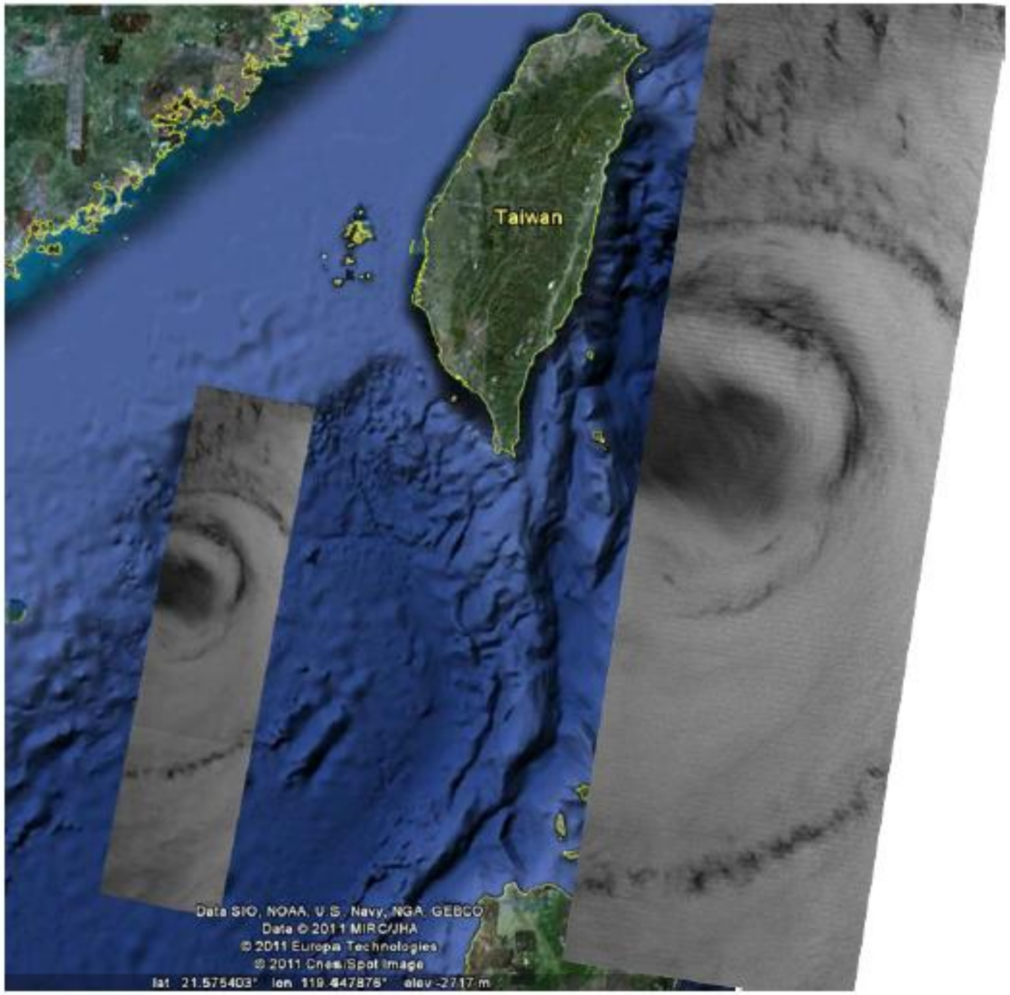

TS-X ScanSAR mode data acquired over the typhoon Megi on October 21, 2010 at 22:06 UTC.

terrasar-x.dlr.de/papers_sci.../OCE0143_li.pdf

Tropical cyclones at SAR images

Announcement of Opportunity: RADARSAT Hurricane Applications Project

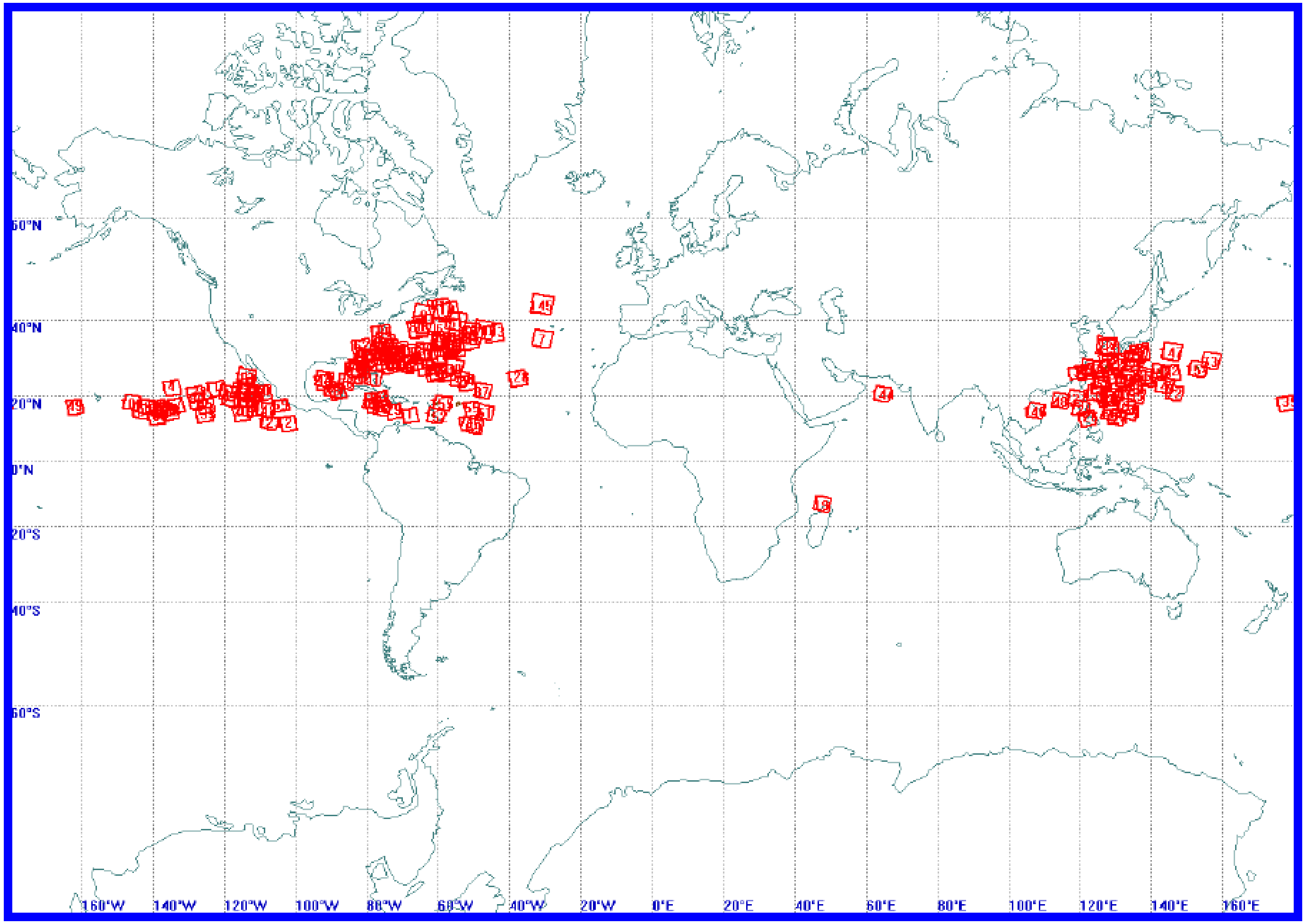

Approximate Locations of the 160 pre-processed images Included in the RADARSAT-1 Hurricane AO Database

Tropical cyclones at SAR images

Schematic plot of tropical cyclone structure and atmospheric phenomena including eye/eyewall, rainband, boundary layer rolls, arc cloud, and mesovortices

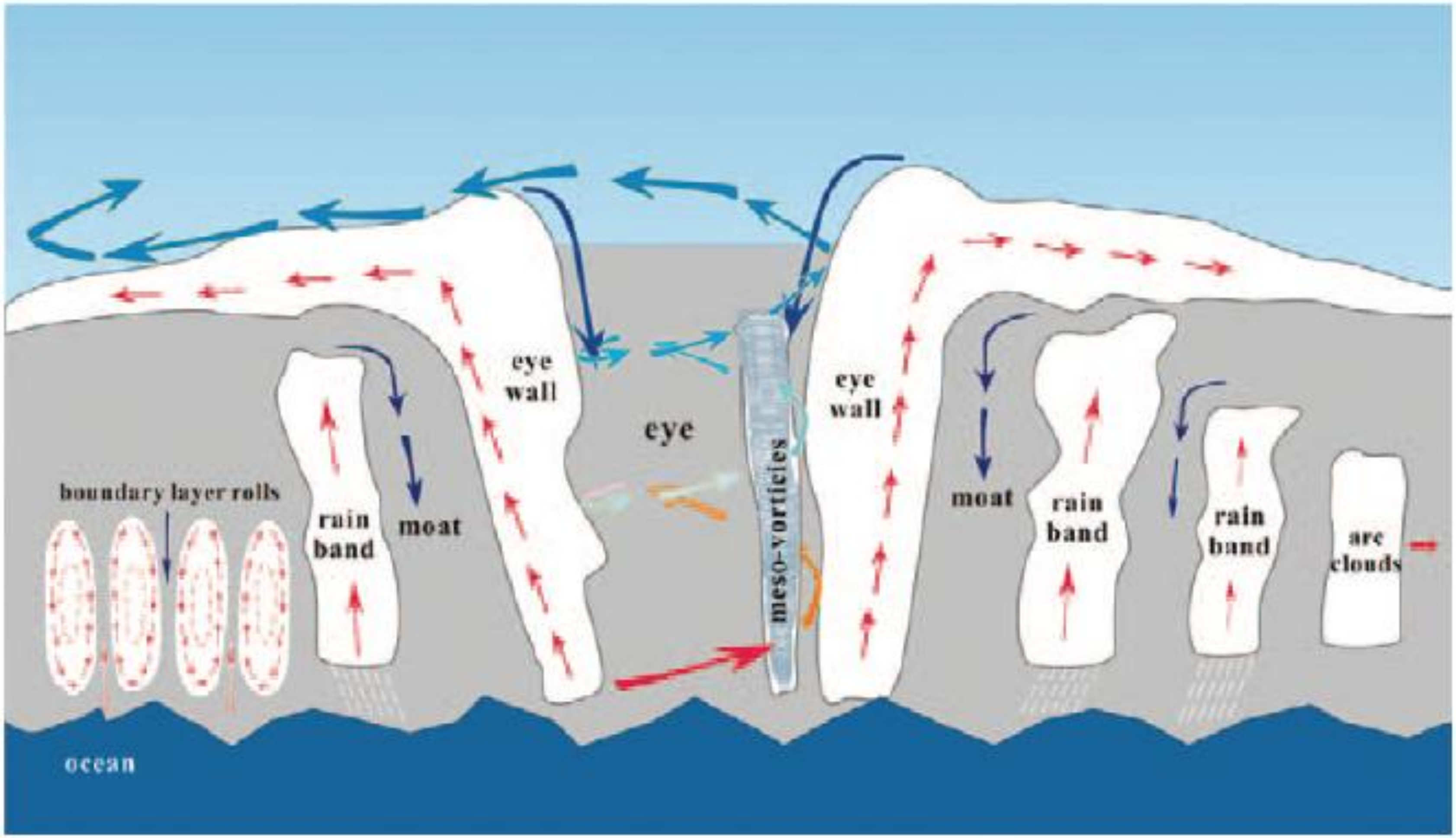

X.Li, J.A. Zhang, X.Yang, W.G. Pichel, M.DeMaria, D.Long, Z. Li Tropical Cyclone Morphology from Spaceborne Synthetic Aperture Radar BAMS, 2013

Tropical cyclones at SAR images

Examples of SAR hurricanes with different eye shapes.

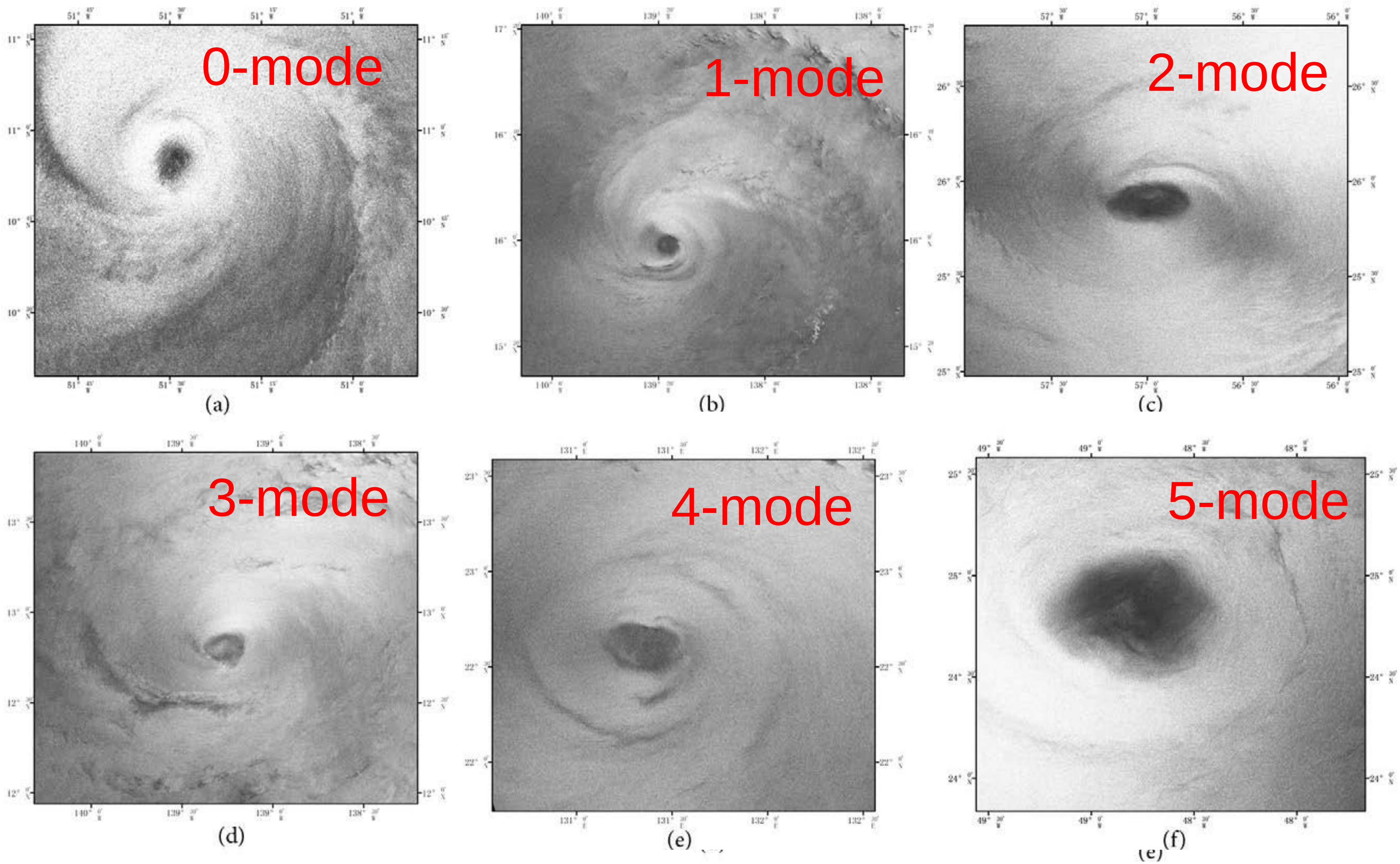

X.Li, J.A. Zhang, X.Yang, W.G. Pichel, M.DeMaria, D.Long, Z. Li Tropical Cyclone Morphology from Spaceborne Synthetic Aperture Radar BAMS, 2013

Tropical cyclones at SAR images

Hurricane eye/eyewall mesovortices.

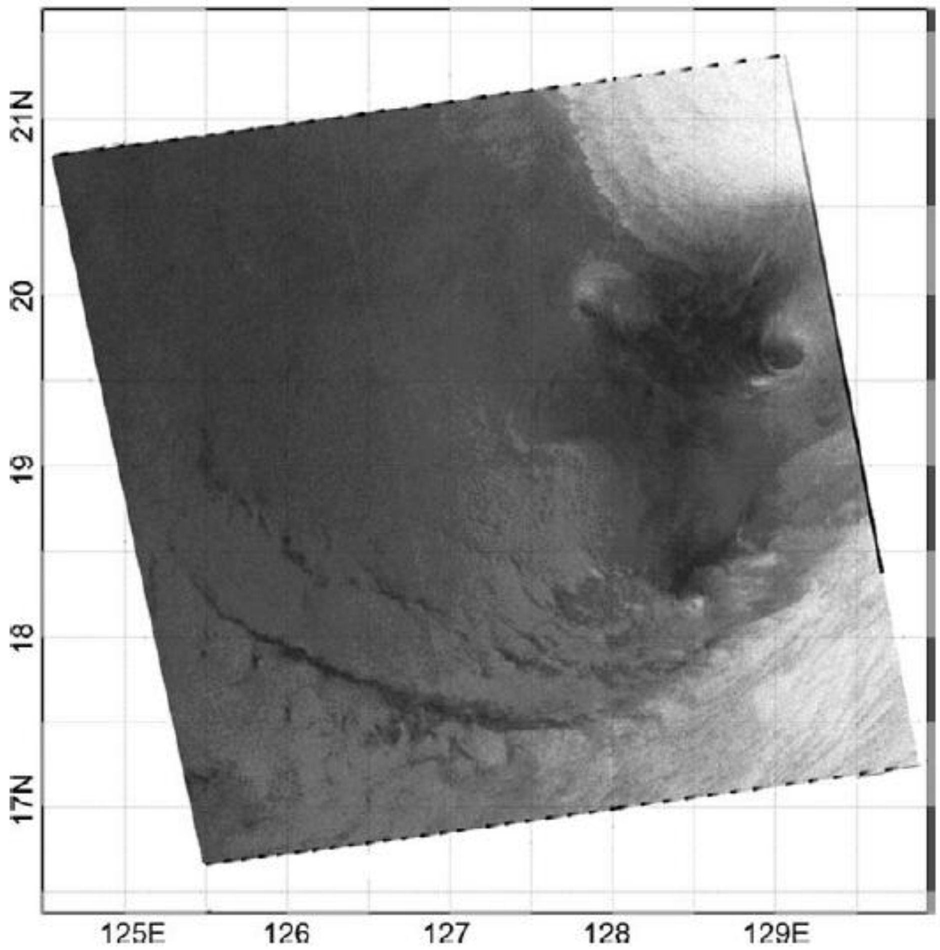

X.Li, J.A. Zhang, X.Yang, W.G. Pichel, M.DeMaria, D.Long, Z. Li Tropical Cyclone Morphology from Spaceborne Synthetic Aperture Radar BAMS, 2013

Tropical cyclones at SAR images

Rainband patterns observed in SAR images

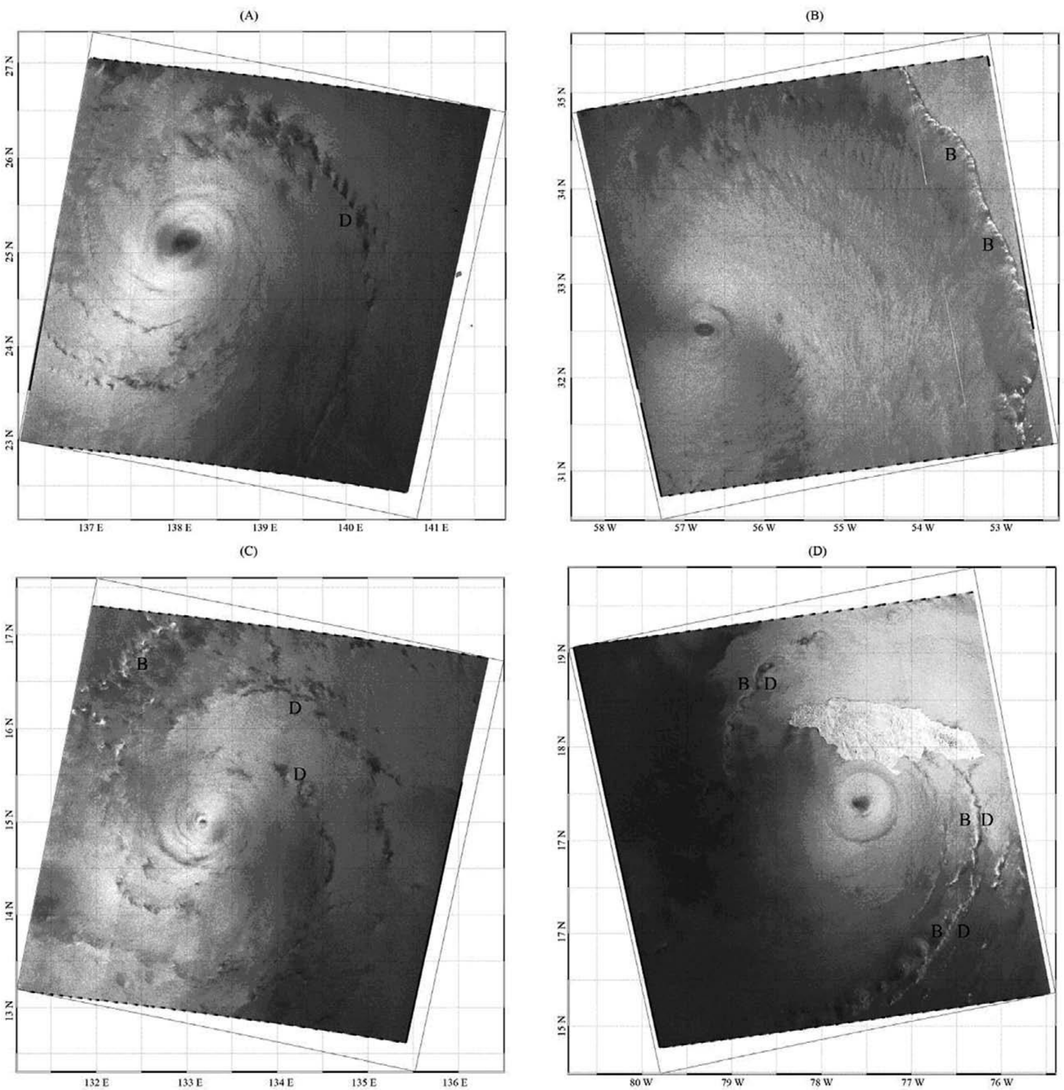

The bright and dark patterns of rainbands are associated with a combination of five physical mechanisms that change the sea surface roughness (e.g., Bliven and Giovanangeli 1993; Lin et al. 2001):

1. attenuation due to heavy rain,
2. backscattering from rain drops in the air and ice particles,
3. sea surface capillary waves induced by rain,
4. damping of sea surface waves by rain-induced turbulence,
5. wind gusts.

X.Li, J.A. Zhang, X.Yang, W.G. Pichel, M.DeMaria, D.Long, Z. Li Tropical Cyclone Morphology from Spaceborne Synthetic Aperture Radar BAMS, 2013

Tropical cyclones at SAR images

Boundary layer rolls within hurricanes

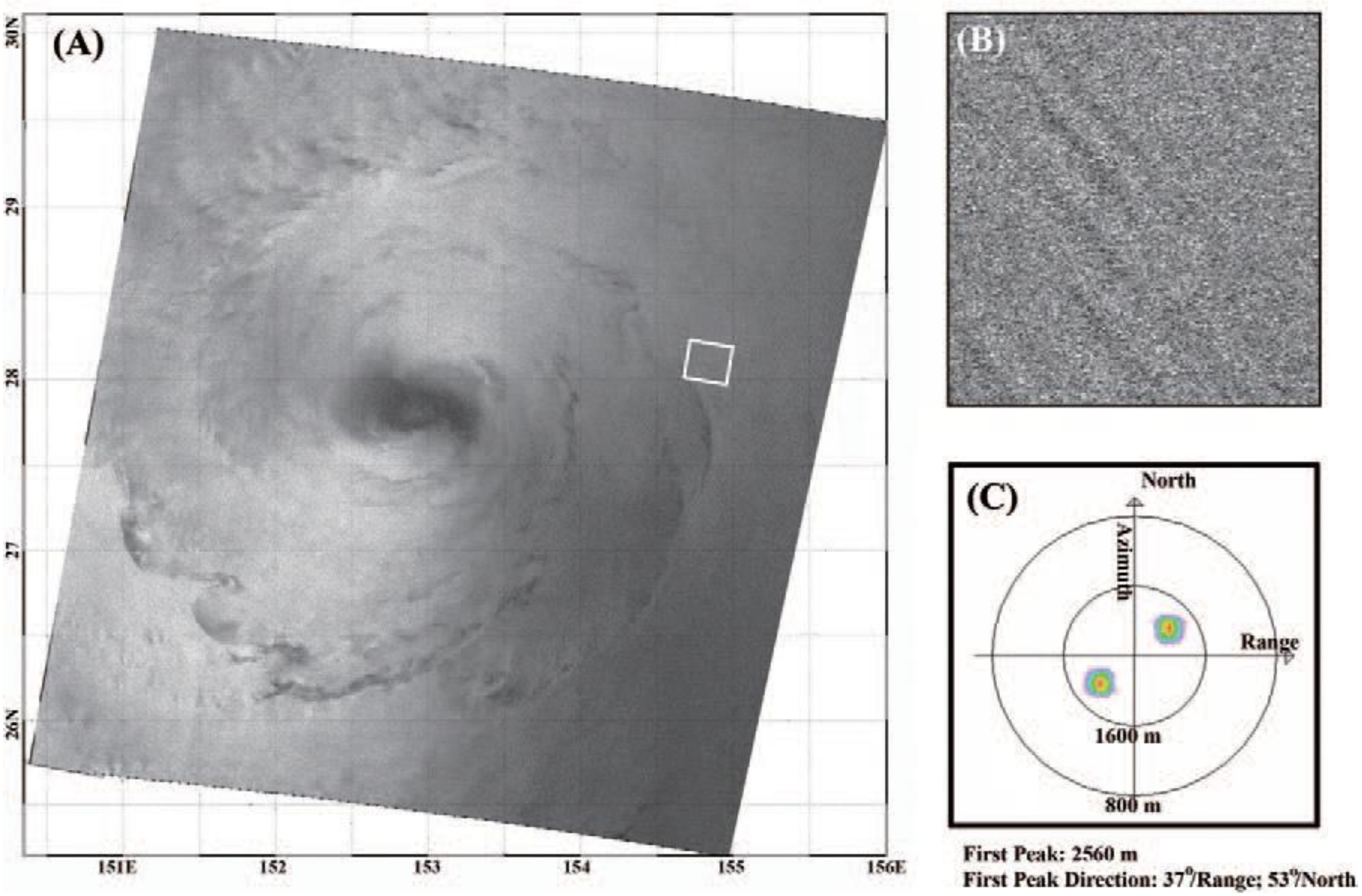

The BL rolls are found to be generally in line with the wind direction. These BL rolls are also related to boundary layer height, as they can be regarded as large eddies expanding the whole boundary layer.

X.Li, J.A. Zhang, X.Yang, W.G. Pichel, M.DeMaria, D.Long, Z. Li Tropical Cyclone Morphology from Spaceborne Synthetic Aperture Radar BAMS, 2013

Tropical cyclones at SAR images

Hurricane patterns over ocean and land observed on SAR images

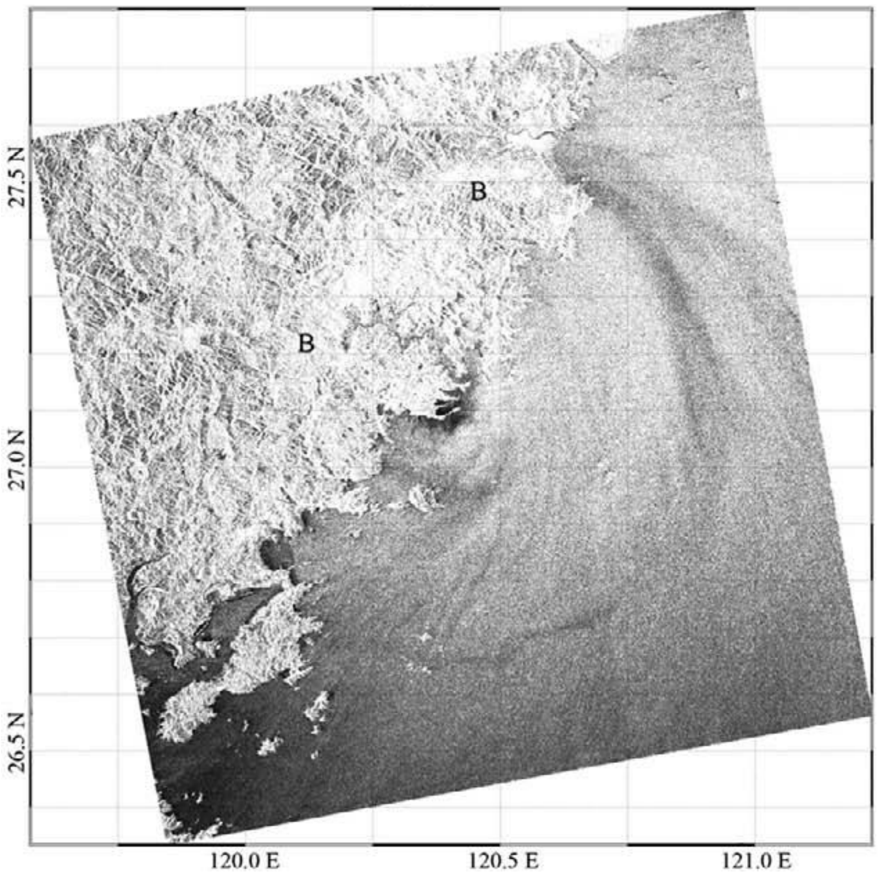

10 August 2006 category 5 Typhoon Saomai image covering the Fujian–Zhejiang coast of China.
The high spiral tropical cyclone wind pattern is visible over ocean. This storm pattern is continuous across the ocean–land boundary and remains the same structure over land. Possibly these NRCS signatures are due to radar scattering and signal attenuation from intense rain in the atmosphere, which is similar over land and ocean.

X.Li, J.A. Zhang, X.Yang, W.G. Pichel, M.DeMaria, D.Long, Z. Li Tropical Cyclone Morphology from Spaceborne Synthetic Aperture Radar BAMS, 2013

Can we measure hurricane wind speed from the SAR image?

Plot of σ_o derived by the CMOD5 GMF depending on wind speed and wind directions at a fixed incidence angle of 25◦.

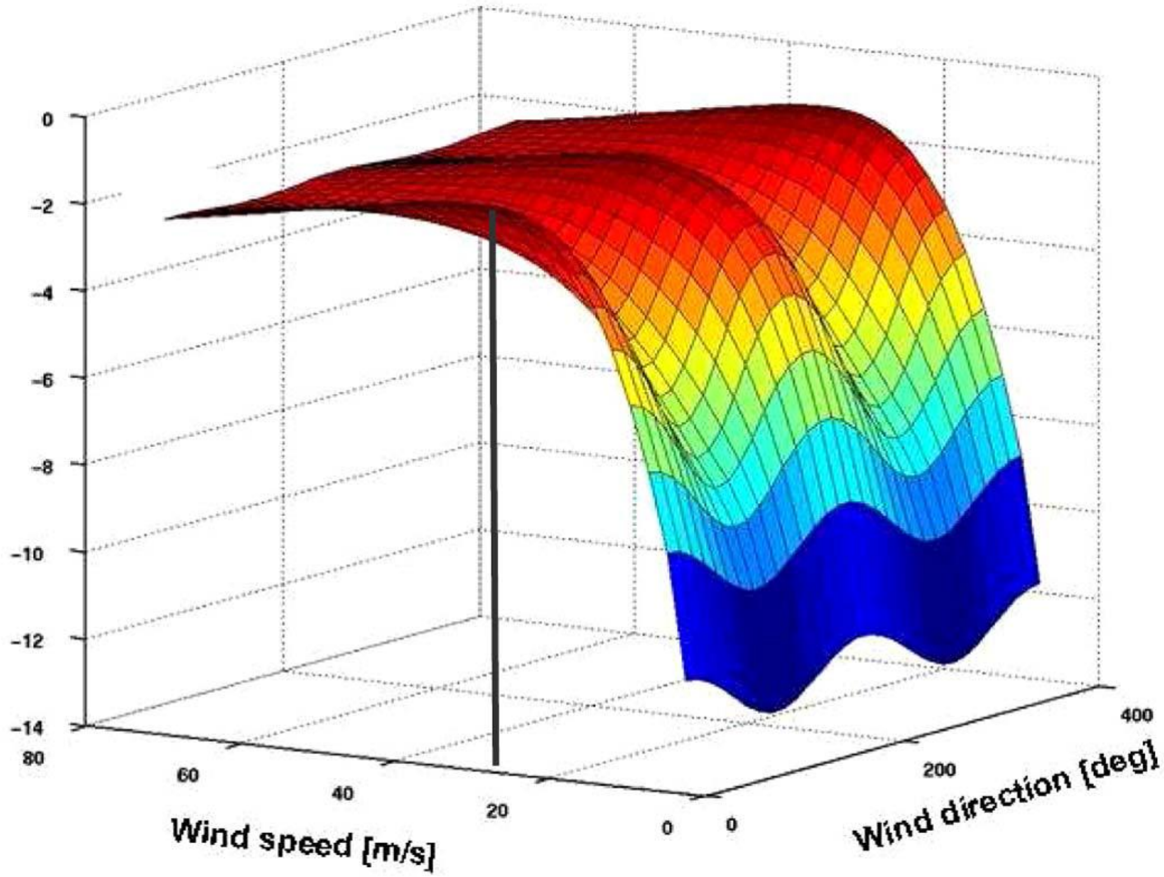

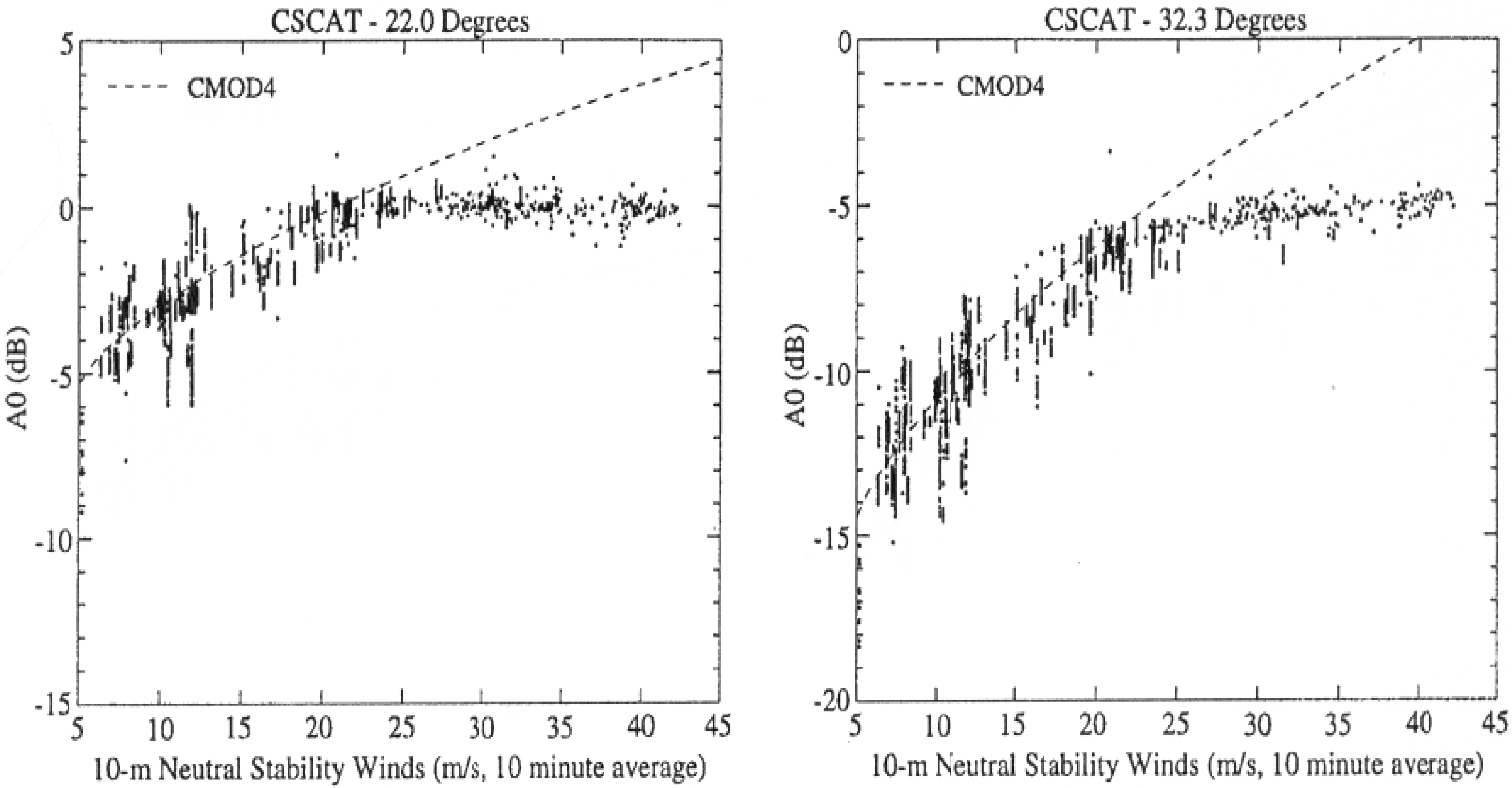

Figure 2. Mean C band normalized radar cross section (NRCS) measurements gathered at (a) 22.0°, (b) 32.3°, (c) 43.5°, and (d) 54.1° incidence plotted versus collocated U_{10N} estimates. The dashed line is the mean NRCS response to the 10-m neutral stability wind speed U_{10N} as predicted by the CMOD4 model function.

MetOp ASCAR

17 October 01:22 UTC

13:12 UTC

Pmin = 895 mb

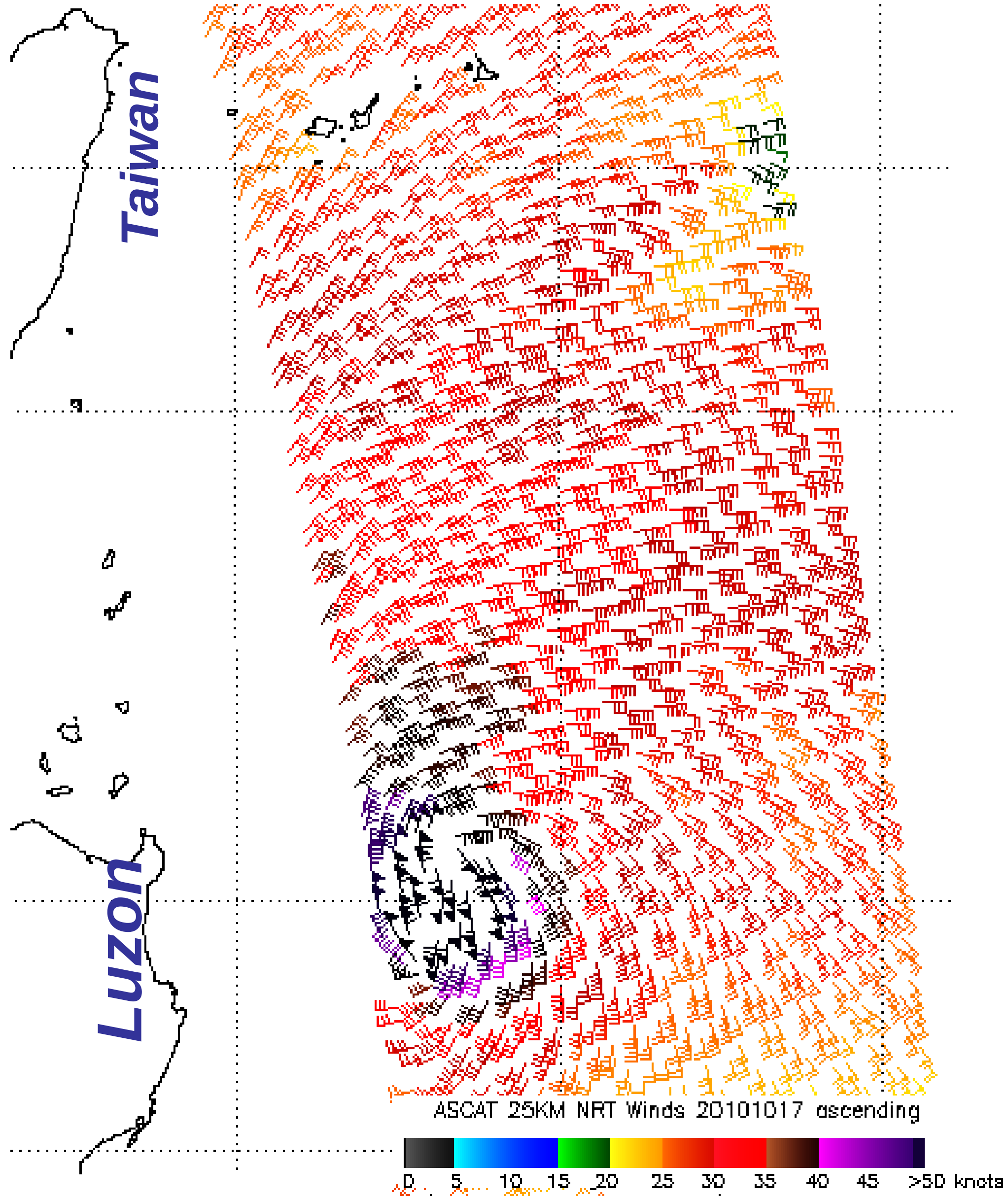

Algorithms CMOD4, CMOD_IFR2, CMOD5 are not applicable for retrieving wind speed exceeding 30 m/s (the problem of ambiguity)

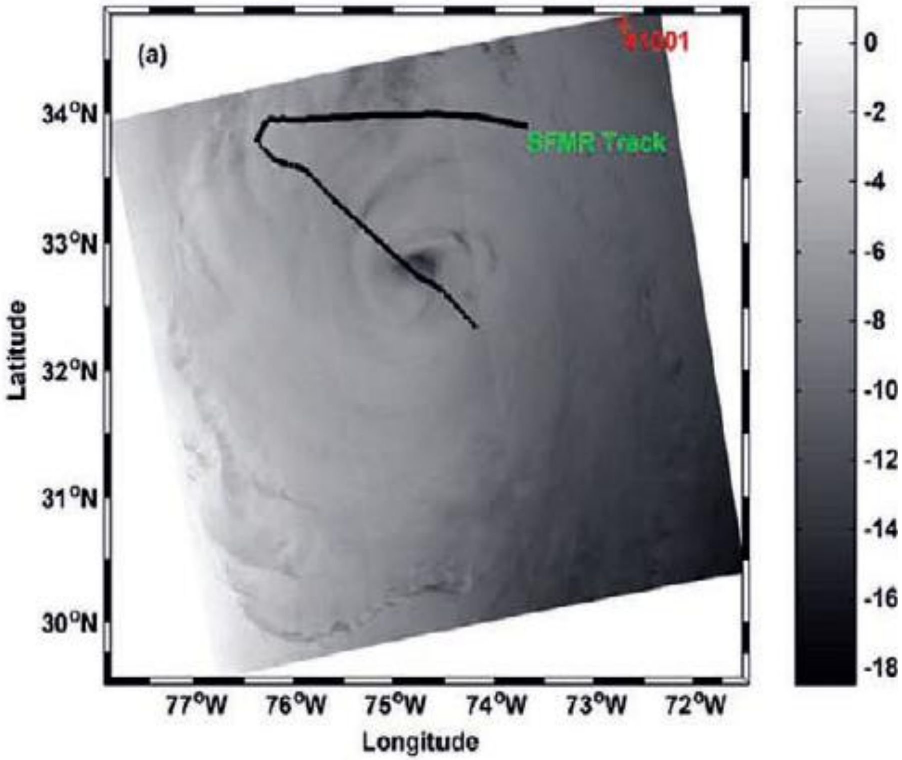

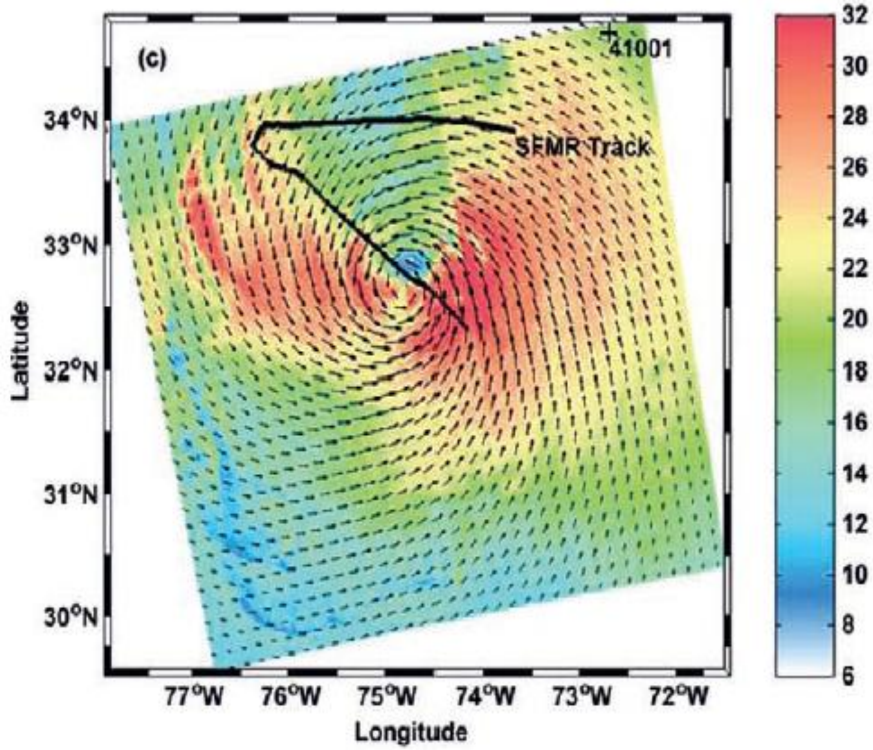

RADARSAT-2 dual-polarization SAR image acquired over Hurricane Earl at 2259 UT C 2 Sep 2010 VV polarization with color bars showing σ_{0VV} in dB, respectively.SAR-retrieved wind speeds from the CMOD 5.N model and σ_{0VV}, with external wind directions from NO AA HRD H*Wind overlaid

B.Zhang, W.Perrie . BAMS, April 2012

Two linear polarizations of electromagnetic waves

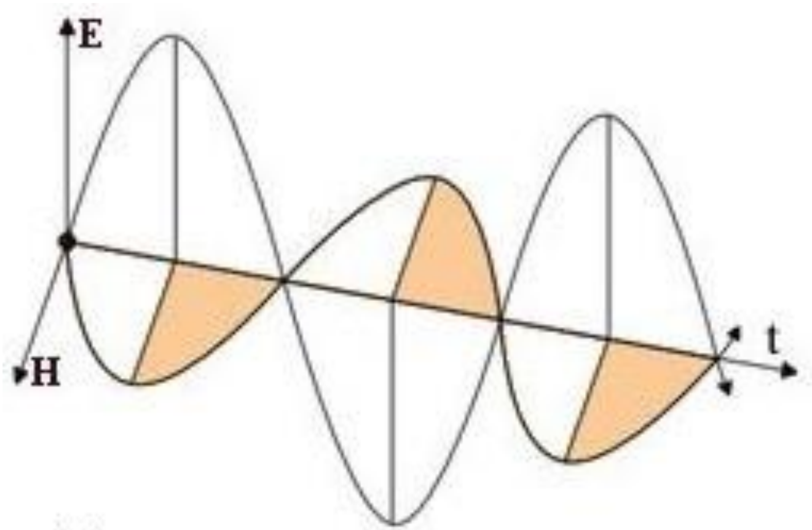

Vertical polarization

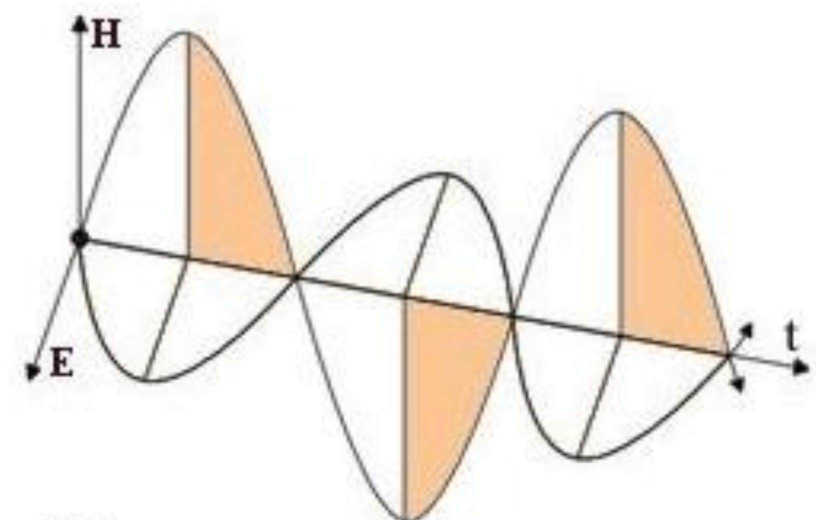

Horizontal polarization

Dependency of co-polarized and de-polarized NRCS of RADARSAT-2 on wind speed

Hwang, P.A, B.Zhang, and W.Perrie, 2010: *Geophys. Res. Lett.*,

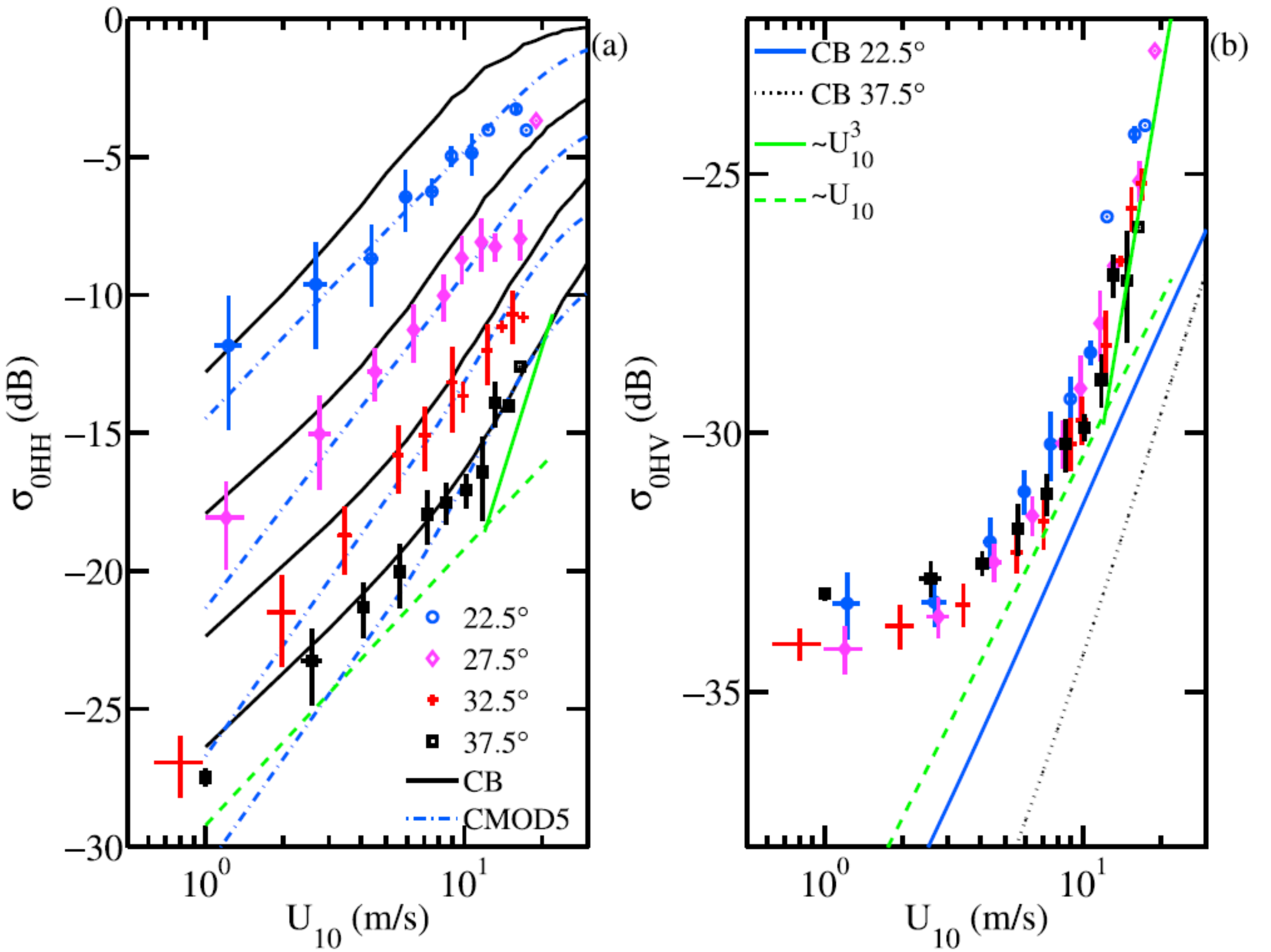

Mean σ_0 vs in situ buoy-measured $U_{10.}$VH polarization

B.Zhang, W.Perrie . BAMS, April 2012

53 NDBC buoy observations of wind and wave collocate 600 RADARSAT-2 Quad-Polarization (HH+VV+HV+VH) images

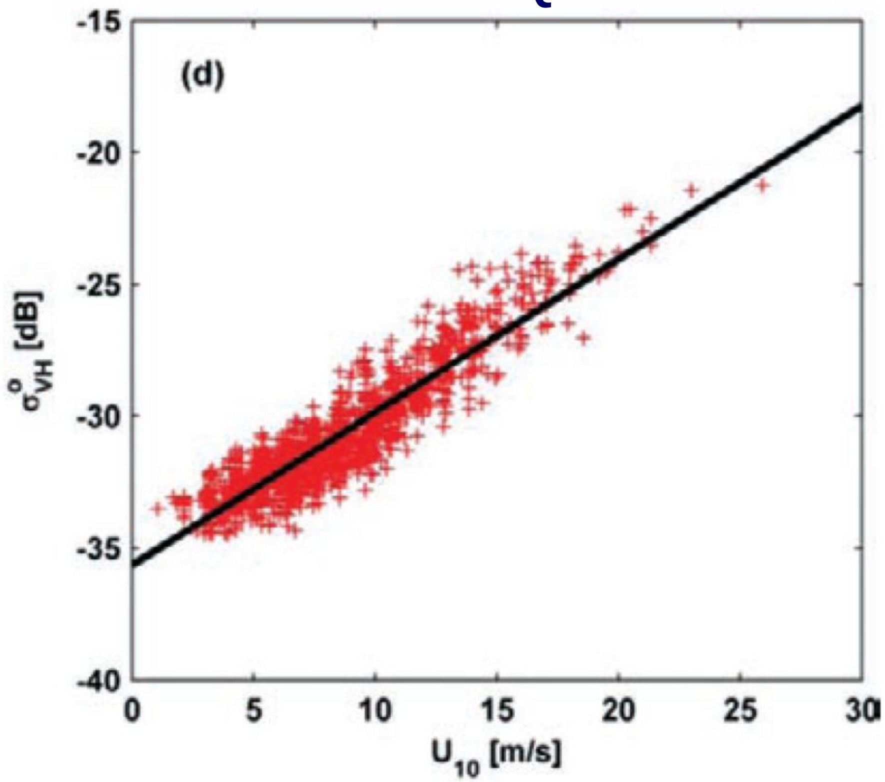

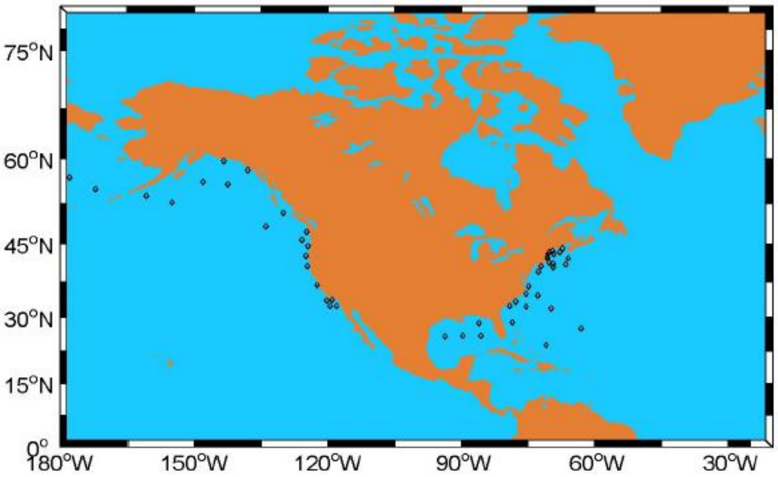

The highest wind speed observation is 26ms^{-1} in these datasets of collocated SAR–buoy measurements

<u>C-2PO model</u>

$$\sigma_{0\mathrm{VH}} = =0.580U_{10} - 35.652$$

Comparing of models CMOD5 and C-2PO for retrieving wind speed in the hurricane Earl (2 September 2010)

B.Zhang, W.Perrie . BAMS, April 2012

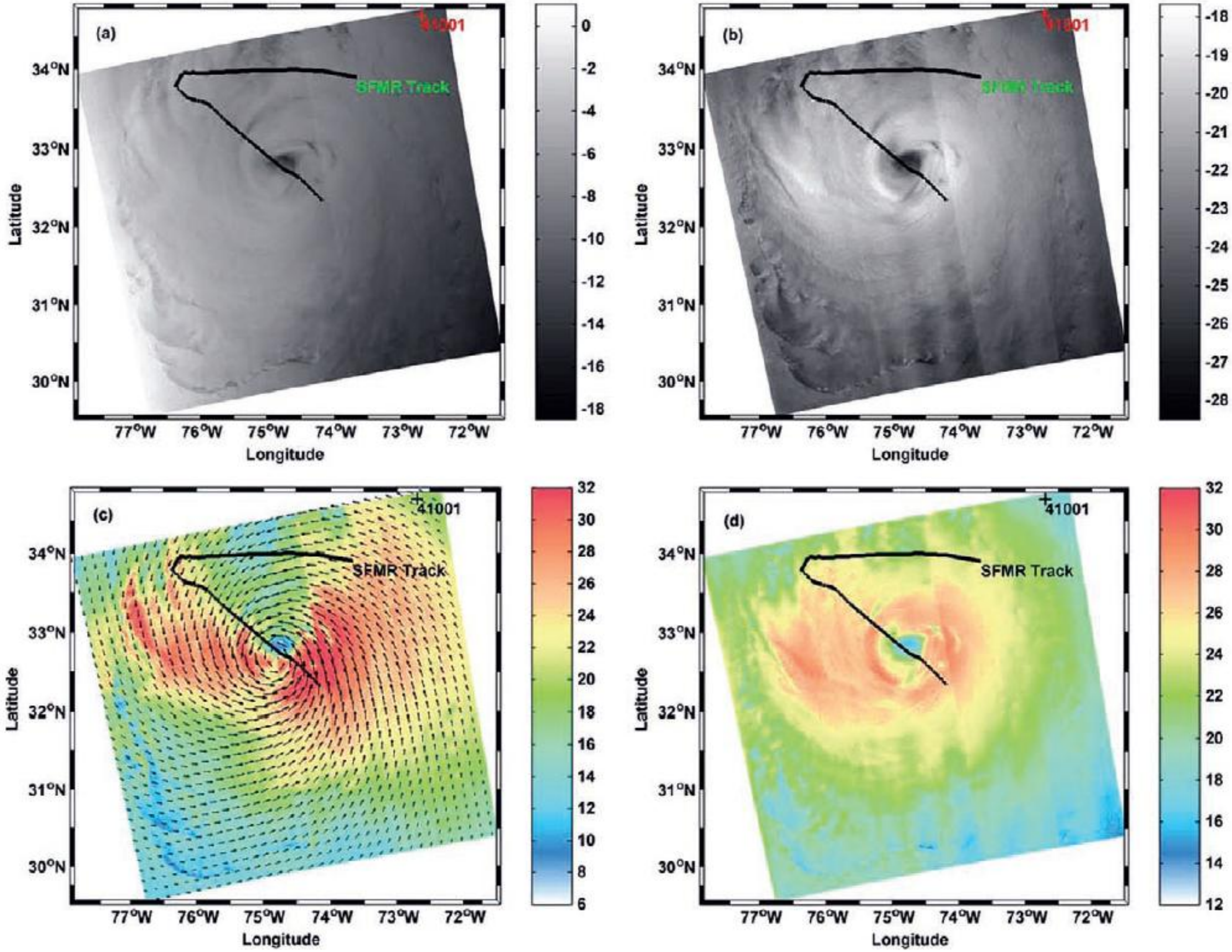

Underestimated wind speed at hurricane conditions (U_{10}>30m/s) as compared wit direct measurements by SFMR (airborne stepped-frequency microwave radiometer)

B.Zhang, W.Perrie . BAMS, April 2012

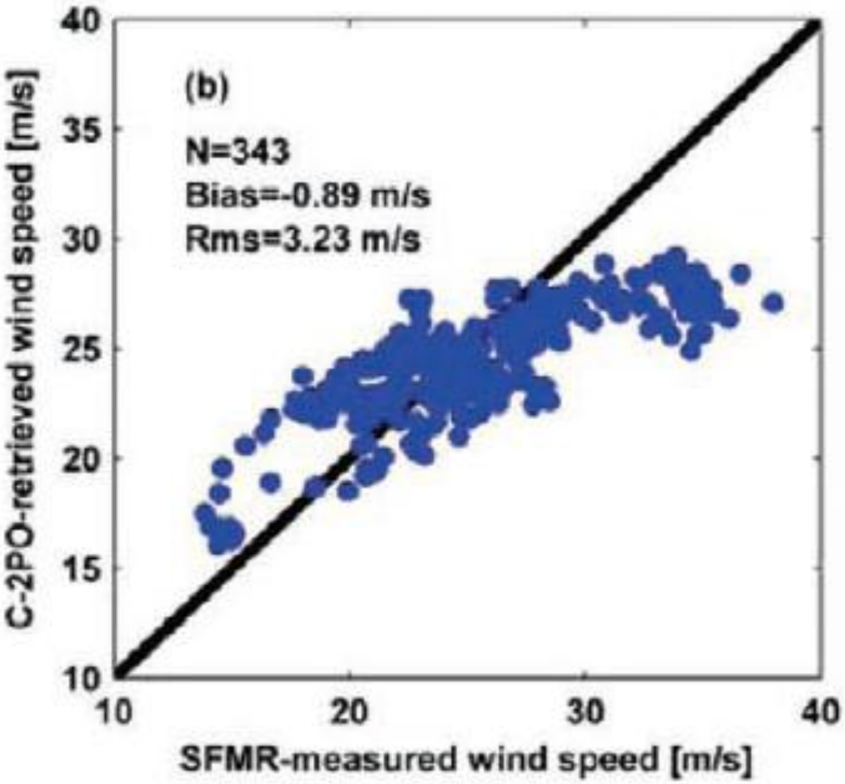

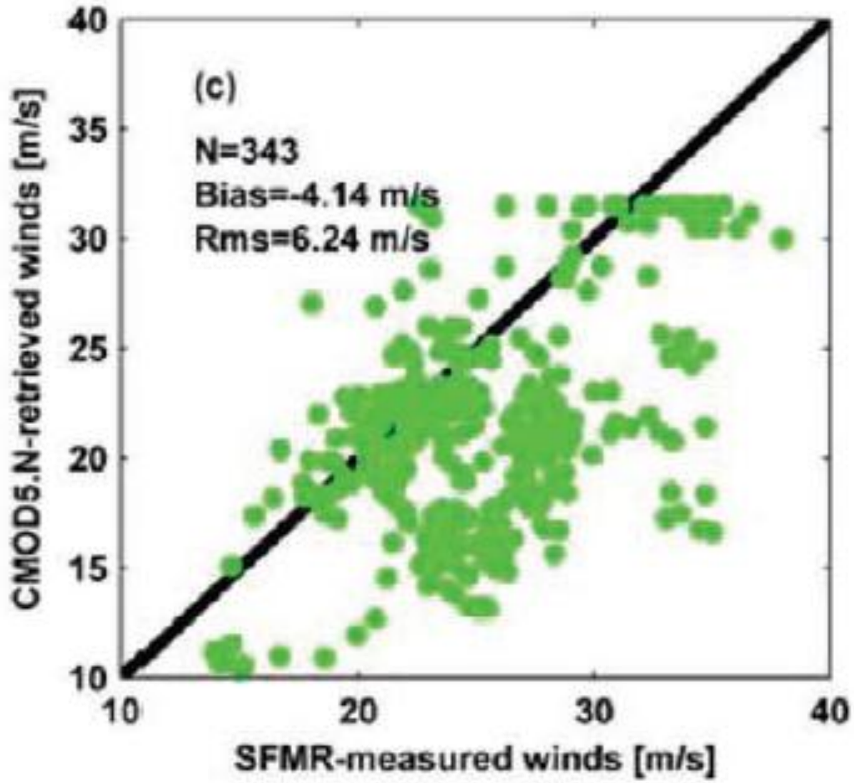

Stepped-frequency microwave radiometer)

The SFMR measures nadir brightness temperature (T_B) at six C-band frequencies, and a retrieval algorithm uses a geophysical model function (GMF) relating surface emissivity and wind speed to produce surface wind speed estimates along the flight track.

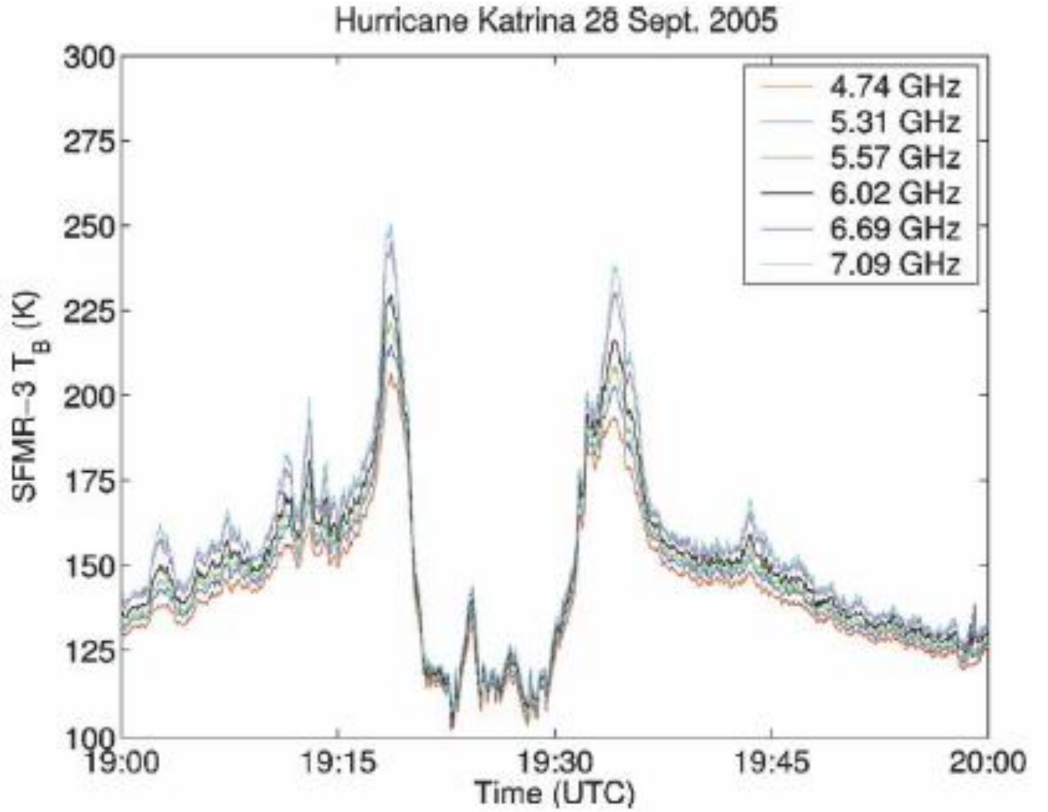

Time series of T_B measurements for each SFMR channel from Hurricane Katrina

Uhlhorn, E. W., and P. G. Black, J. L. Franklin, M. Goodberlet, J. Carswell, A. S. Goldstein, 2007: Hurricane surface wind measurements from an operational stepped frequency microwave radiometer. *Mon. Wea. Rev.,* **135,** 3070–3085.

Wind-induced excess emissivity (ε_w) as a function of U_{sfc} and (right) binned ε_w estimates.

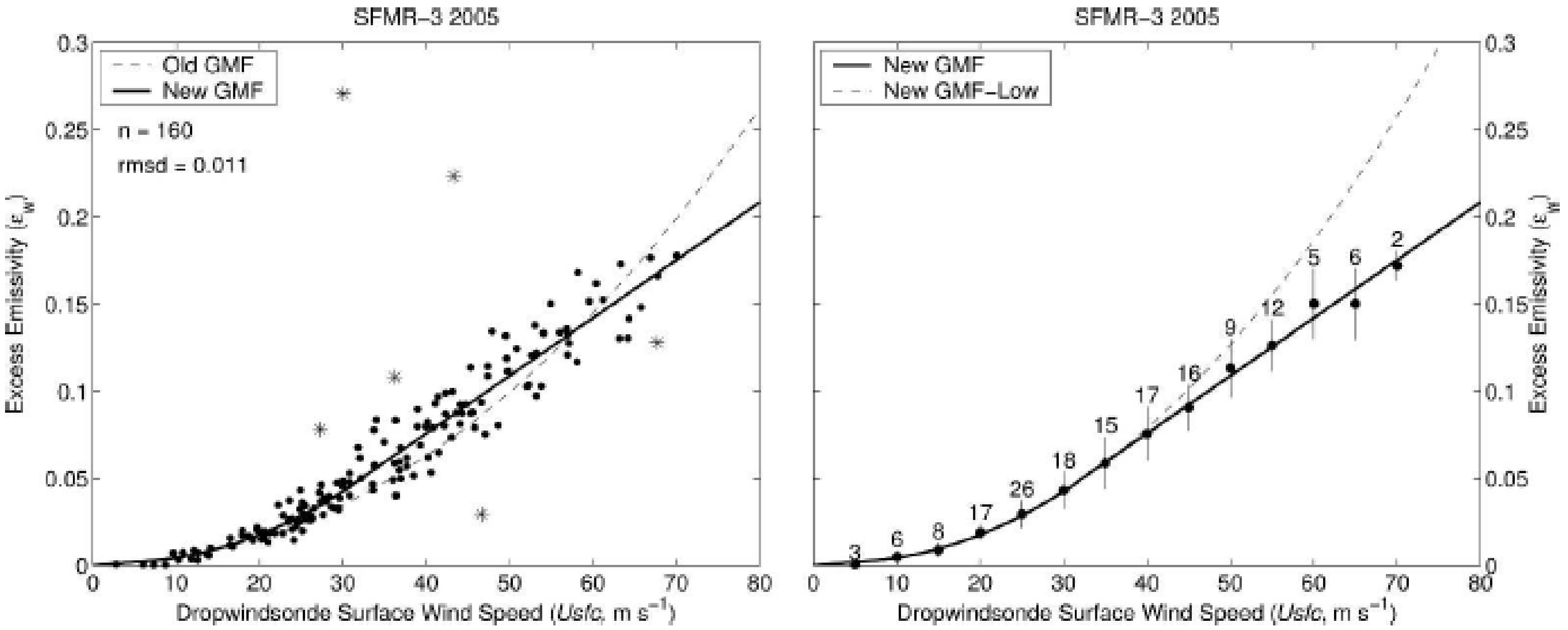

Distribution of all retrieved SFMR wind speeds versus collocated VH measurement points from 9 hurricanes

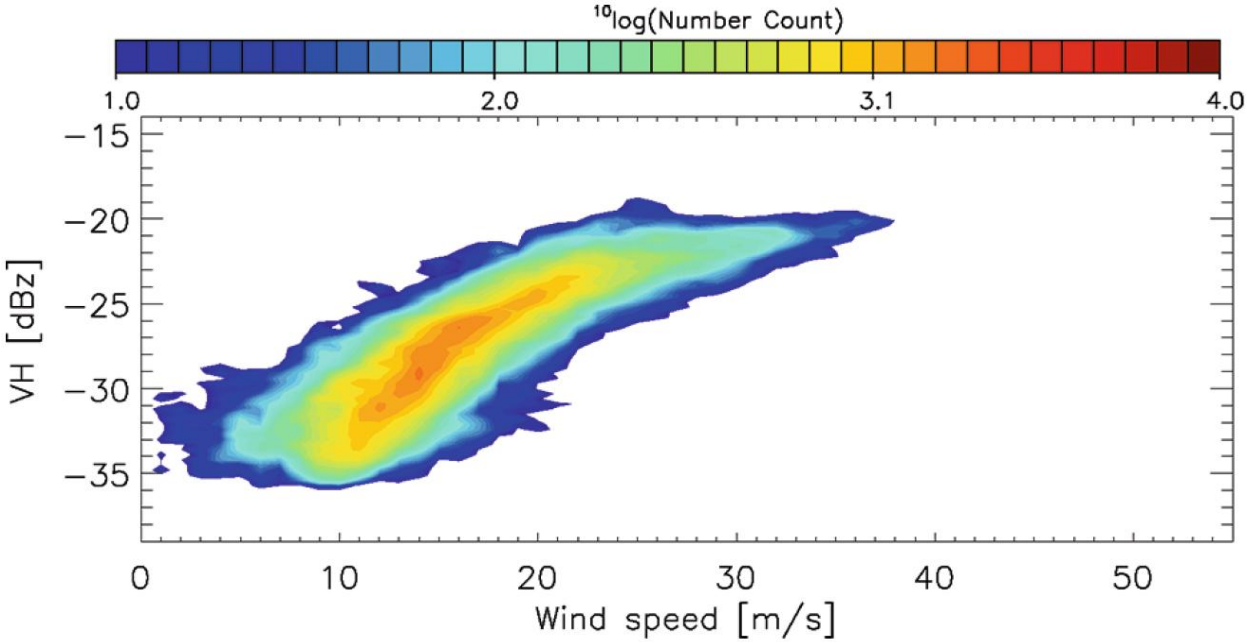

$$\sigma_{VH}^{C} = \begin{cases} -35.6 + 0.58U_{10}\ , \mathit{for}\ U_{10} < 21, \\ -29.1 + 0.22U_{10}\ , \mathit{for}\ 21 < U_{10} < 40. \end{cases}$$

G.-J. van Zadelhoff, A. Stoffelen, P. W. Vachon, J. Wolfe, J. Horstmann, and M. Belmonte Rivas Scatterometer hurricane wind speed retrievals using cross polarization. Atmos. Meas. Tech. Discuss., 6, 7945–7984, 2013

Retrieved SFMR wind speeds from a flight track through hurricane Earl (black line). The blue line depicts the collocated VH RADARSAT-2 measurements

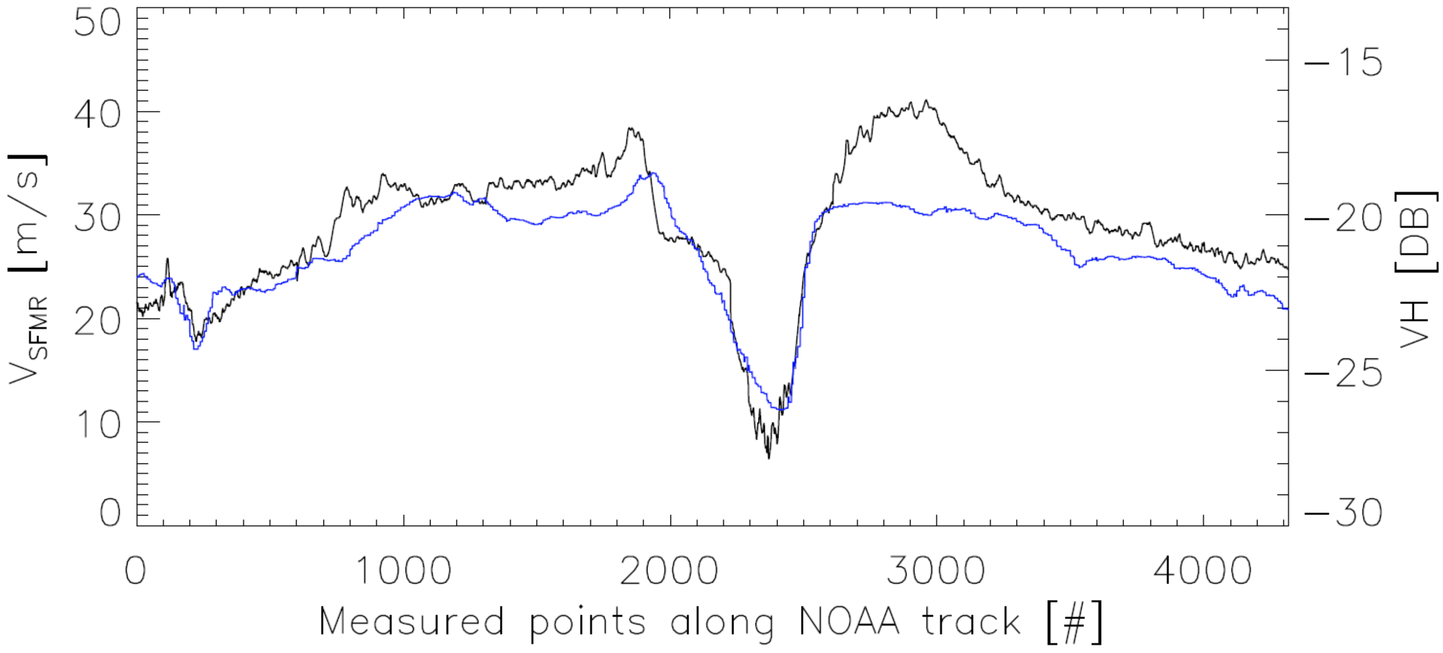

G.-J. van Zadelhoff, A. Stoffelen, P. W. Vachon, J. Wolfe, J. Horstmann, and M. Belmonte Rivas Scatterometer hurricane wind speed retrievals using cross polarization. Atmos. Meas. Tech. Discuss., 6, 7945–7984, 2013

C-band scatterometer for new Meteorological Operational satellite programme Second Generation (MetOp-SG) will be equipped with additional beam operating at cross-polarization.

The purpose of this work

-**To get insight of physical processes responsible for the de-polarized radar return**

- **To obtain the functional dependence of cross-polarized radar cross-section on the wind speed instead of the statistical dependency obtained by collocation of RADARSAT-2 imaginary with approximate collocation with airborne SFMR measurements**

The Large Thermostratified Test Tank with high-speed wind-wave flume

overall dimensions 20m x 4m x 2 m

(L20xW4xD2)m3, 3 refrigerating machines , 6 pump unit

Pc ~ 130 000 Kcal/hour

Max. temperature gradient ~ 1.0-1.5 0C/cm

The fan and overall view of wind-wave flume

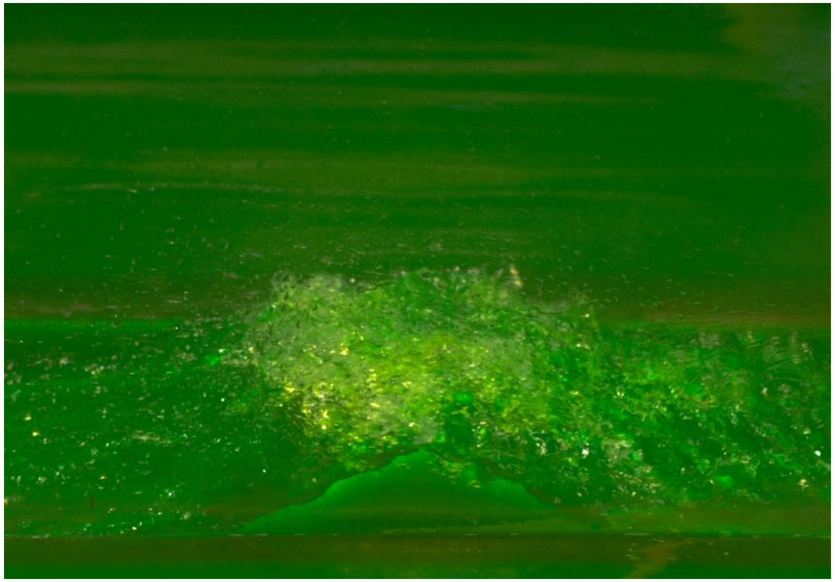

•Dimensions of the channel 10m x 0.4m x 0.4 m

•centerline airflow 3 - 25 m/s

•equivalent 10-m neutral wind speed U_{10} 4 - 40 m/s,

Wind – wave at U_{10}=40 m/s

Pitot gauge and MKS Baratron 226 AD

c)

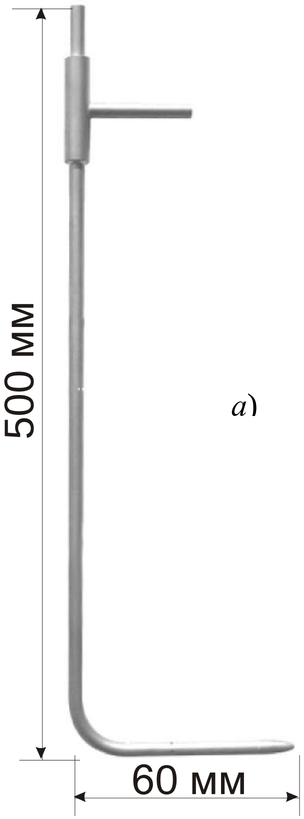

a)

b)

Wind wave field parameters

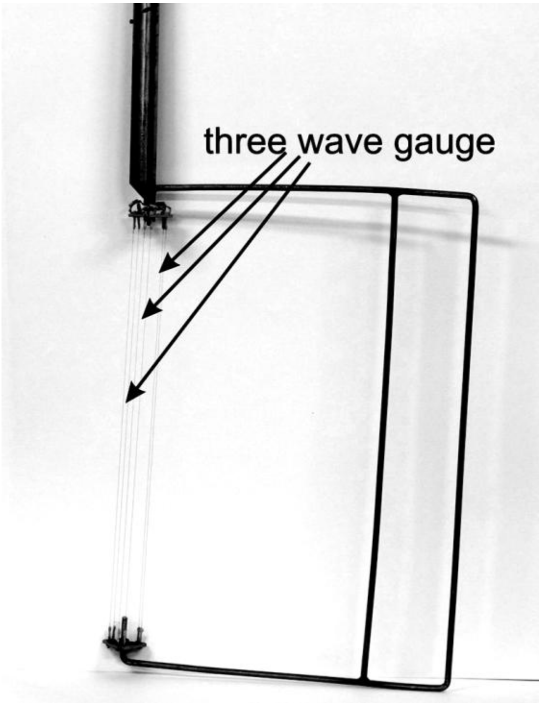

Retrieved from measurements by 3 channel wire gauges positioned in angles of an equal-side triangle, each side is 2.5 cm. Maximum wave number ku=1.25cm^{-1} is prescribed by the size of the triangle.

Data sampling rate was 100 Hz.

3D frequency-wave-number spectra were calculated by Fourier directional method (FDM)

(a modification of WDM, Donelan et al, 1994)

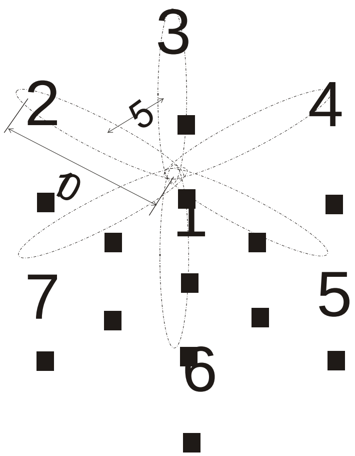

6-channel wire wave-gauge, base 0.7 cm.

Corresponds to $k_{Bragg}/3$

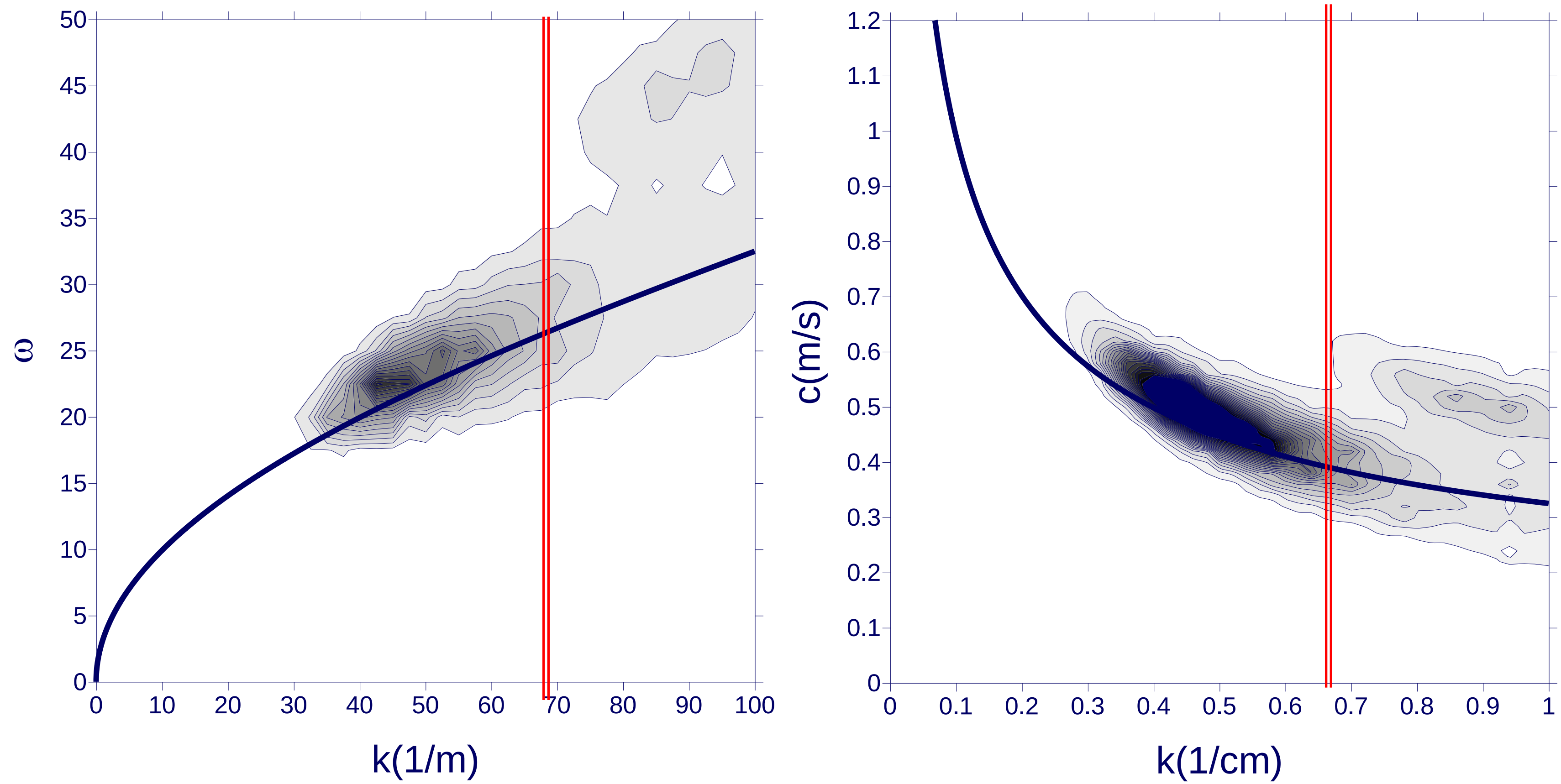

Изолинии двумерных спектров насыщения на плоскости частота-волновое число (а, в, д, ж) и на плоскости фазовая скорость – волновое число (б, г, е, з) для скоростей ветра на высоте 10 м 12.4 м/с.

Corresponds to $k_{Bragg}/3$

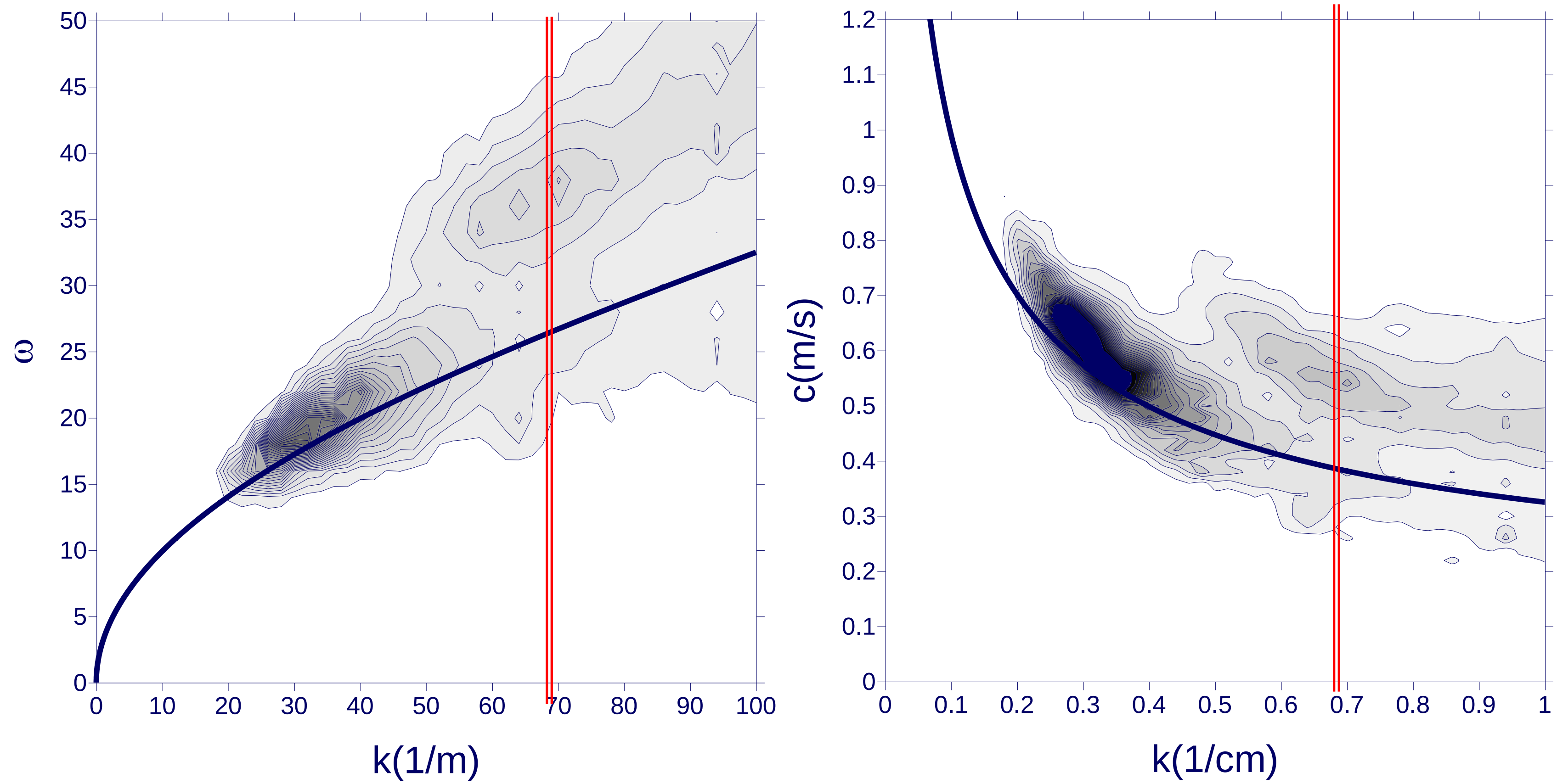

Изолинии двумерных спектров насыщения на плоскости частота-волновое число (а, в, д, ж) и на плоскости фазовая скорость – волновое число (б, г, е, з) для скоростей ветра на высоте 10 м 17.5 м/с.

Corresponds to $k_{Bragg}/3$

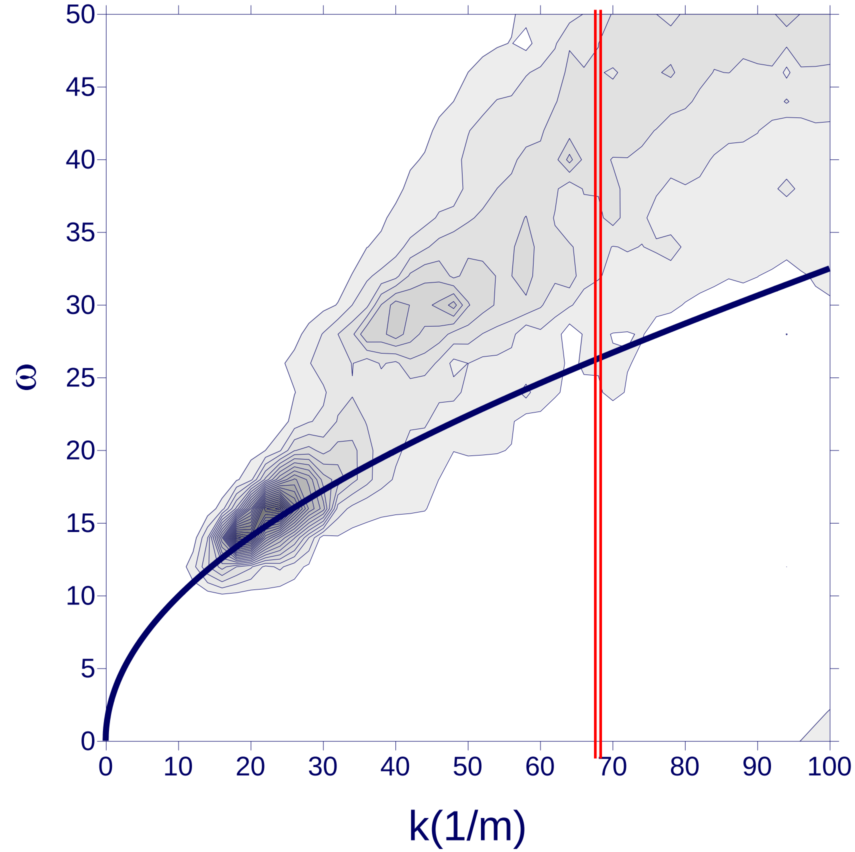

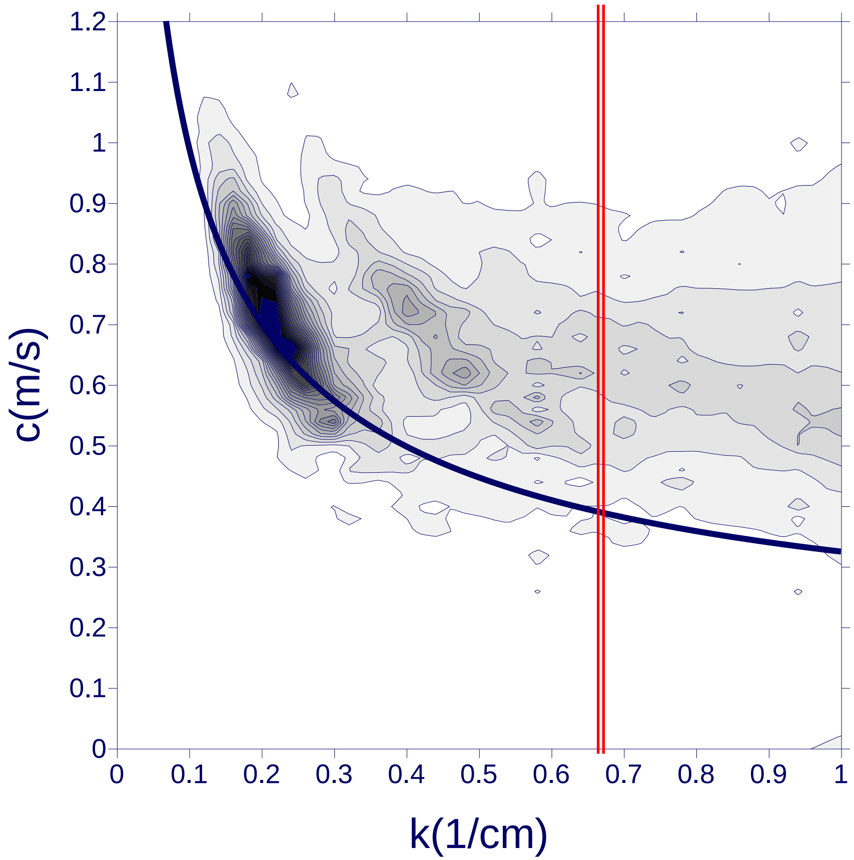

Изолинии двумерных спектров насыщения на плоскости частота-волновое число (а, в, д, ж) и на плоскости фазовая скорость – волновое число (б, г, е, з) для скоростей ветра на высоте 10 м 25.0 м/с.

Corresponds to $k_{Bragg}/3$

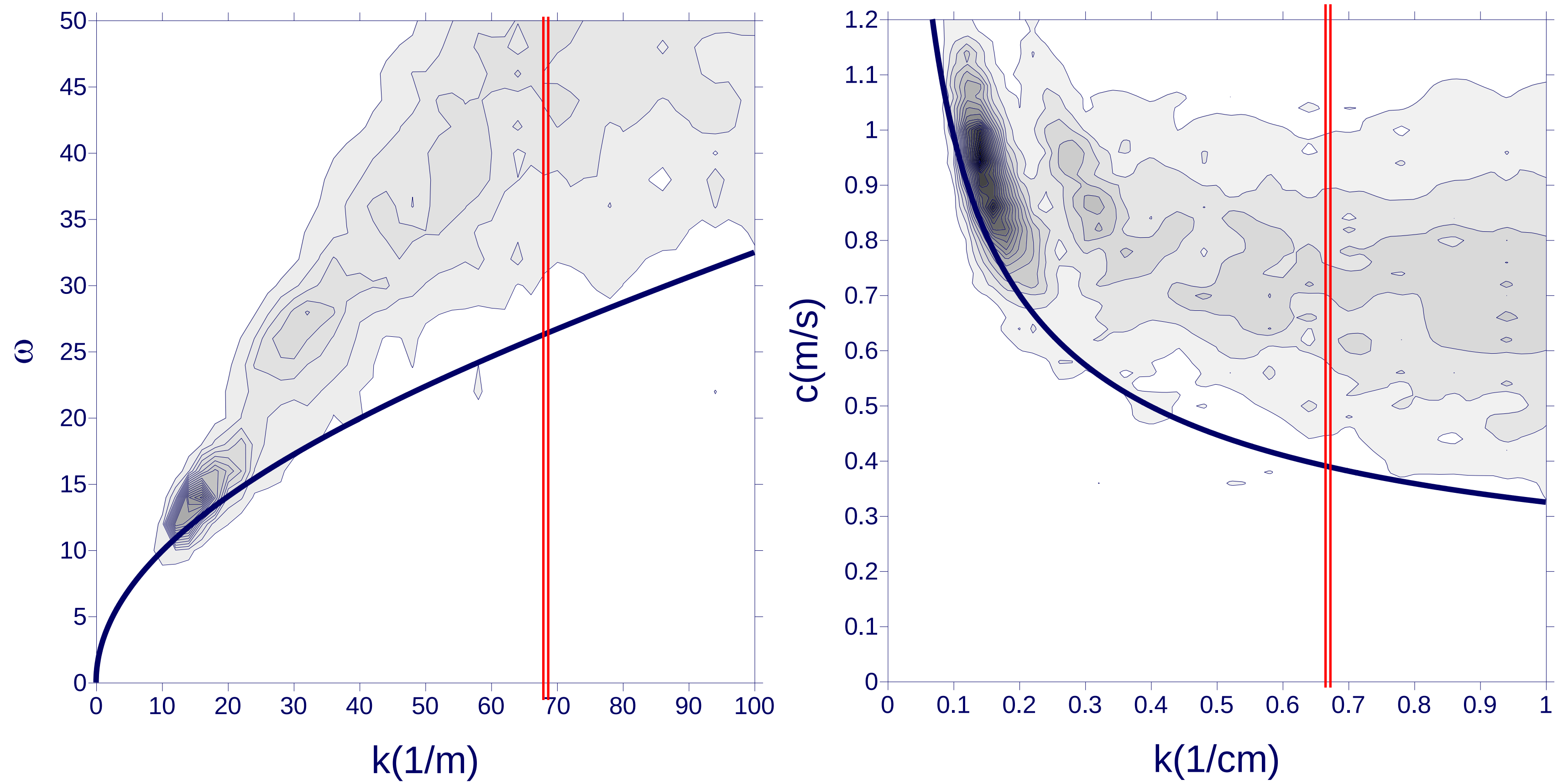

Изолинии двумерных спектров насыщения на плоскости частота-волновое число (а, в, д, ж) и на плоскости фазовая скорость – волновое число (б, г, е, з) для скоростей ветра на высоте 10 м 31.4 м/с.

Omnidirectional phase velocity spectra of surface waves a) total spectrum, b) waves with k>1 cm^{-1}

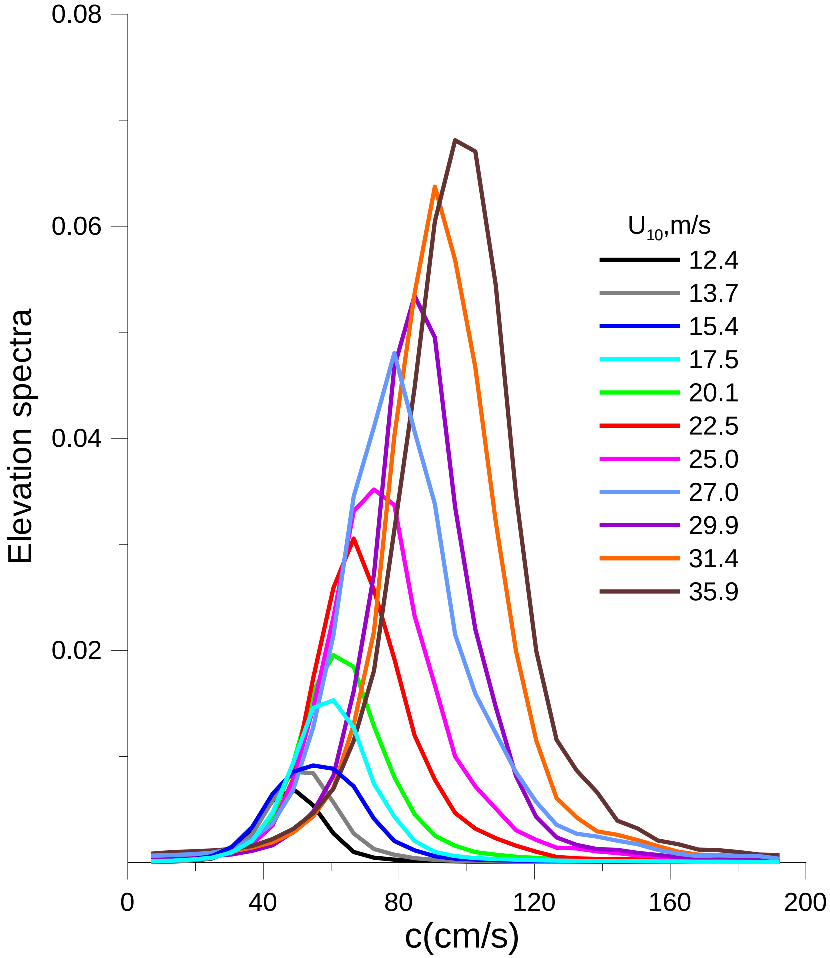

(a)

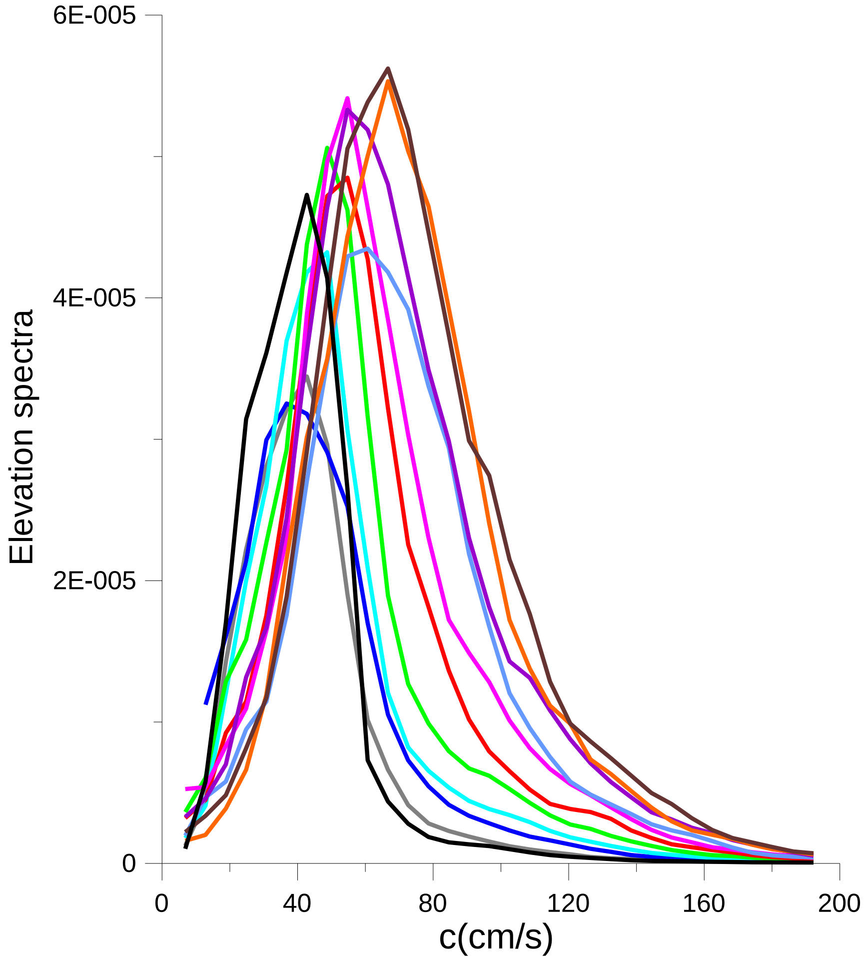

(b)

Slope probability density function

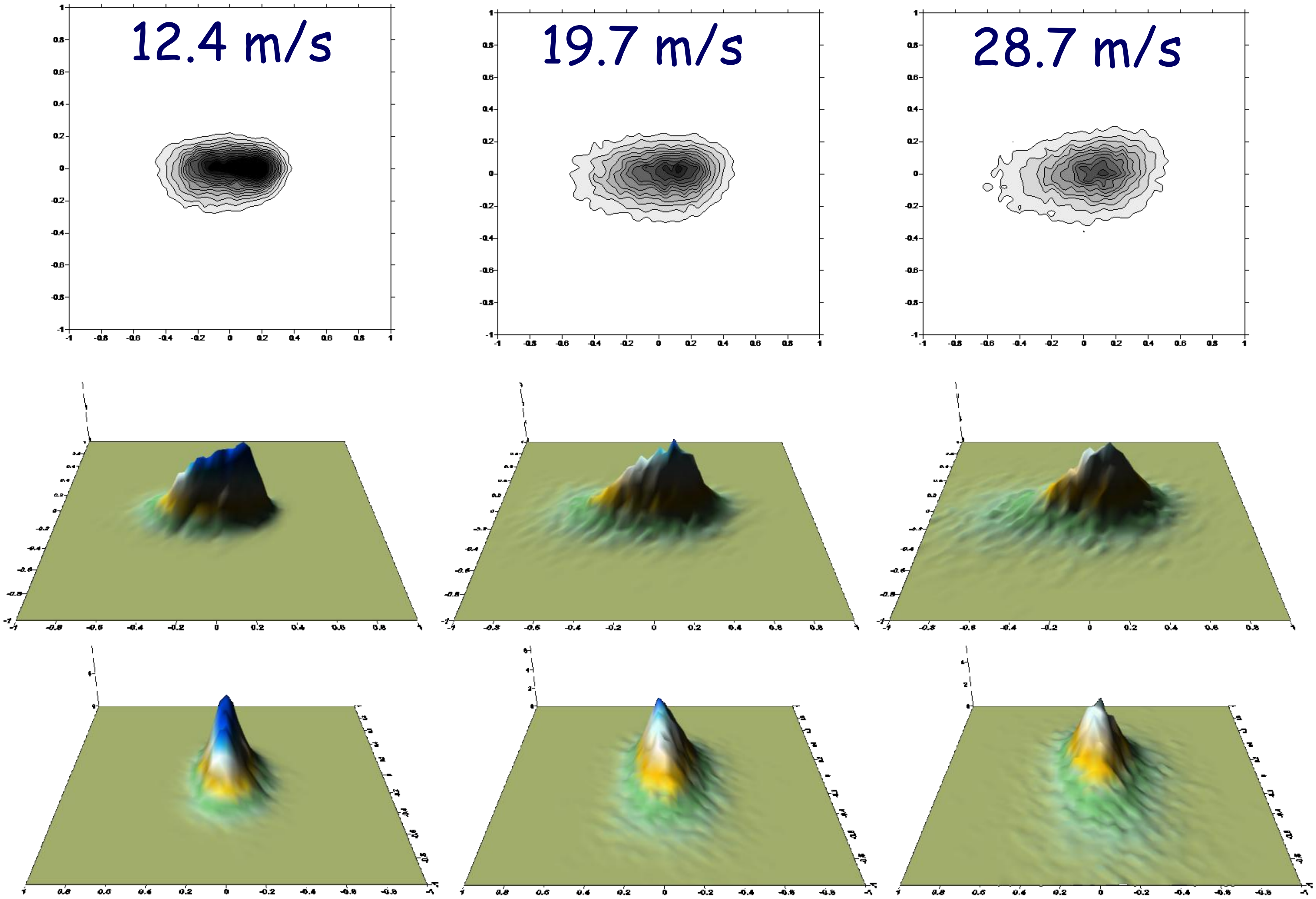

Short wave spectra

6-channel wire wave-gauge, base 0.7 cm.

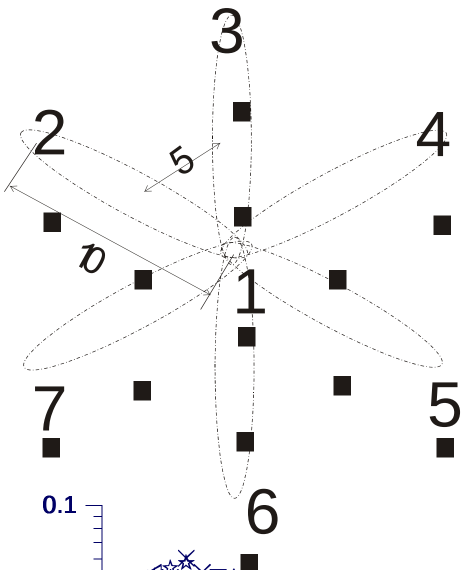

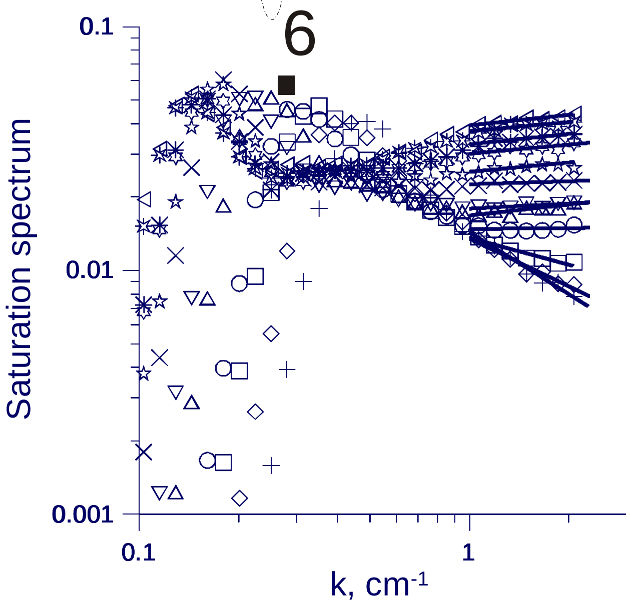

Omnidirectional saturation spectrum for k>1 cm^{-1}

$$B = \alpha k^{\beta}$$

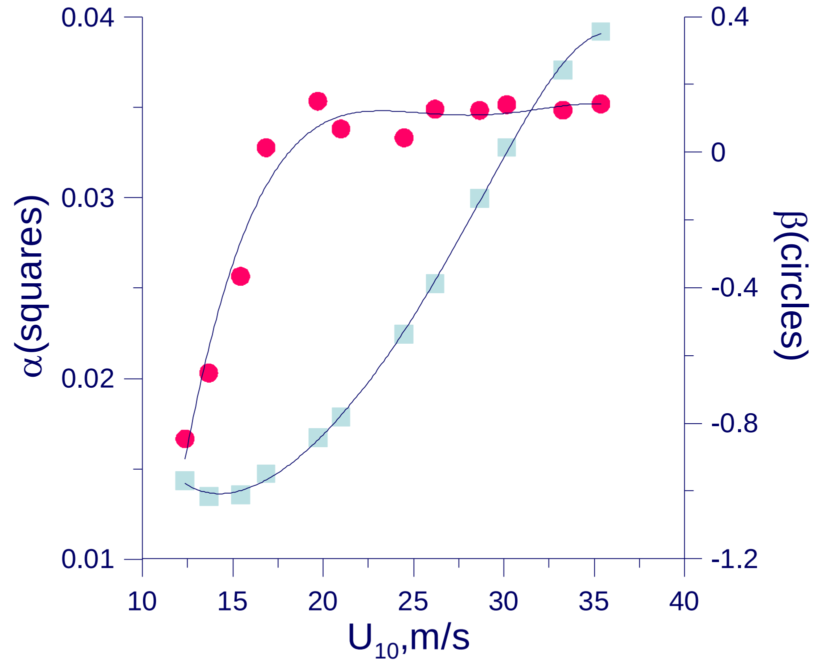

Scheme of the experiment

<u>Conditions of the experiment:</u>

the size of the observation window – 40x40 cm

Incidence angle 30 deg looking upwind

Distance from the target – 3.16m (height 2.75 m from the water)

Thickness of the plexiglas of the flume – 8.3mm

<u>Scaterometer</u>

X-band (3.2 cm)
Polarizations:
VV, HH, VH, HV
Antenna is a pyramidal horn with square cross-section.
The beam width is 9^o

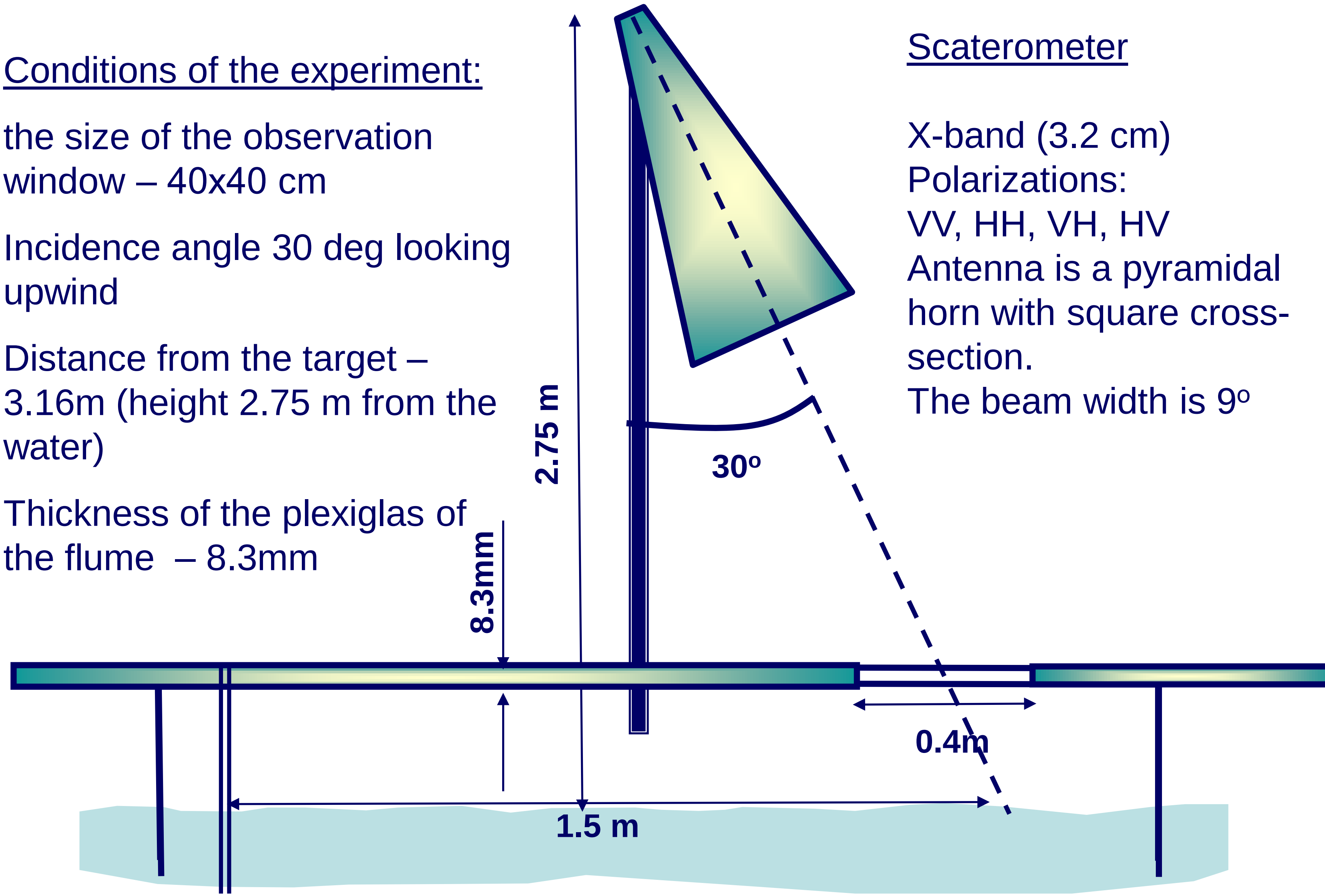

Overall view of the experimental setup and its elements

Photo of microwave tract of
scatterometer

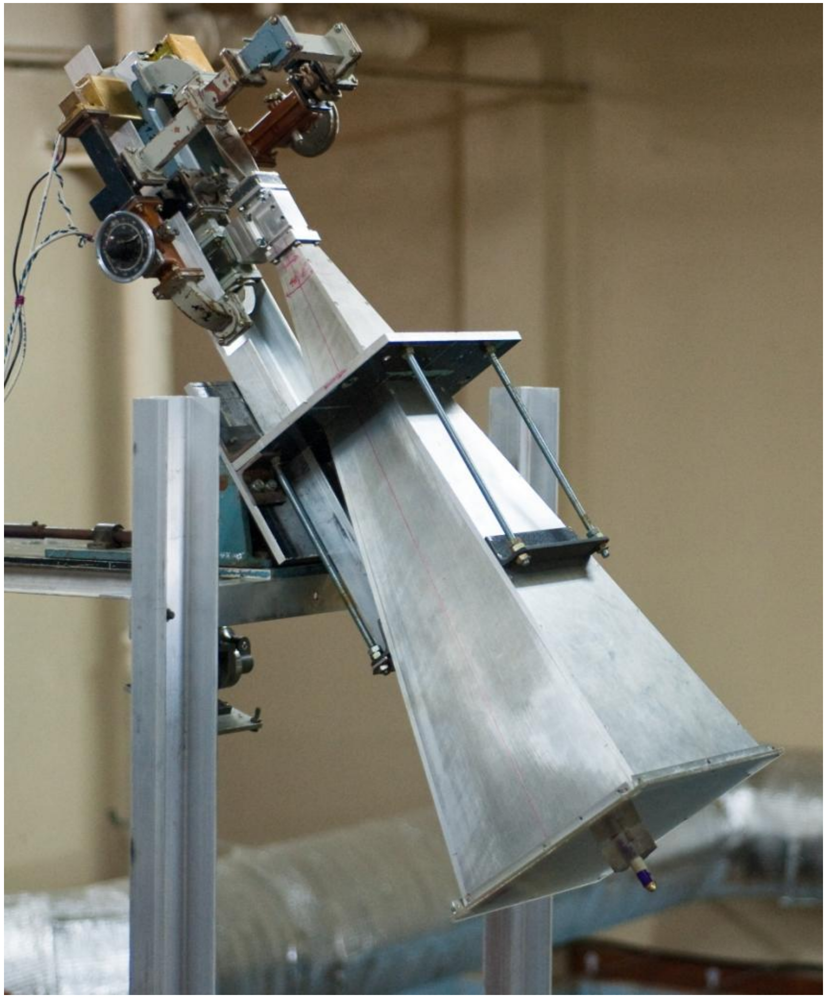

To reduce the influence of reflections taken from the side lobes, the most "critical" reflectors of the tank were covered with pieces of of radio-absorbing material. Structure of the coverage followed the structure of side lobes of rectangular horn - ie cruciform one, corresponding to the main plane of the radiation pattern (ie E-and H-plane).

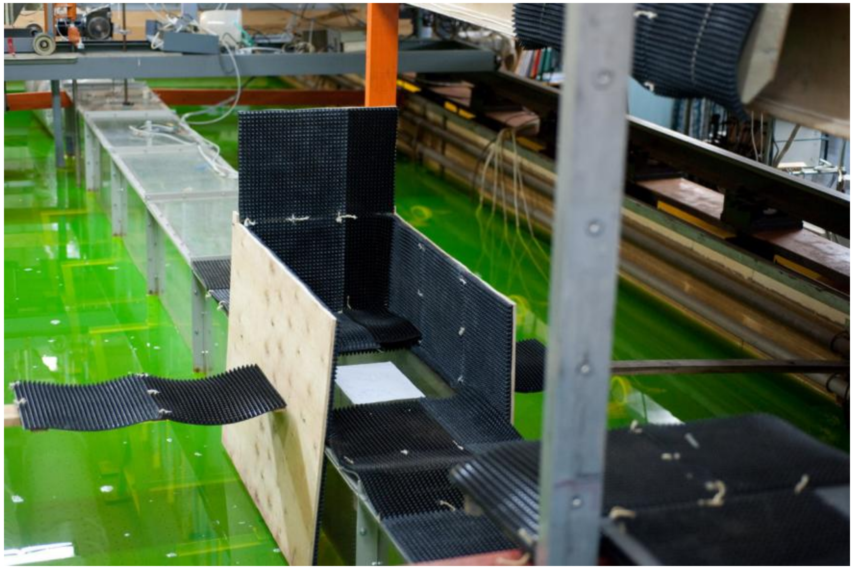

Co-pol and de-pol normalized radar cross sections of water surface as functions of 10-m wind speed, incidence angle 30°

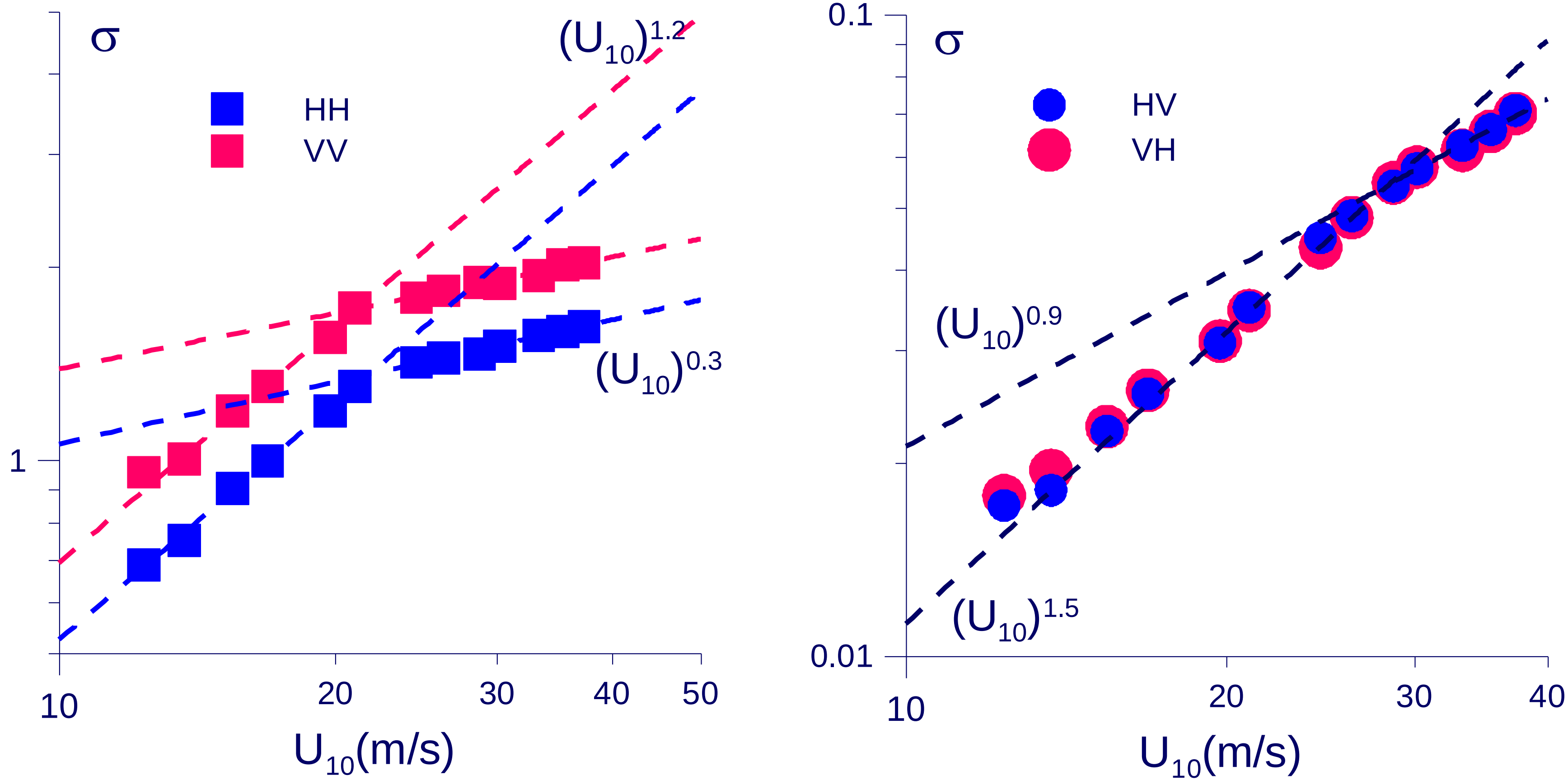

Comparison of measured co-polarized and cross-polarized radar cross-sections and predictions of composite-surface Bragg scattering model.

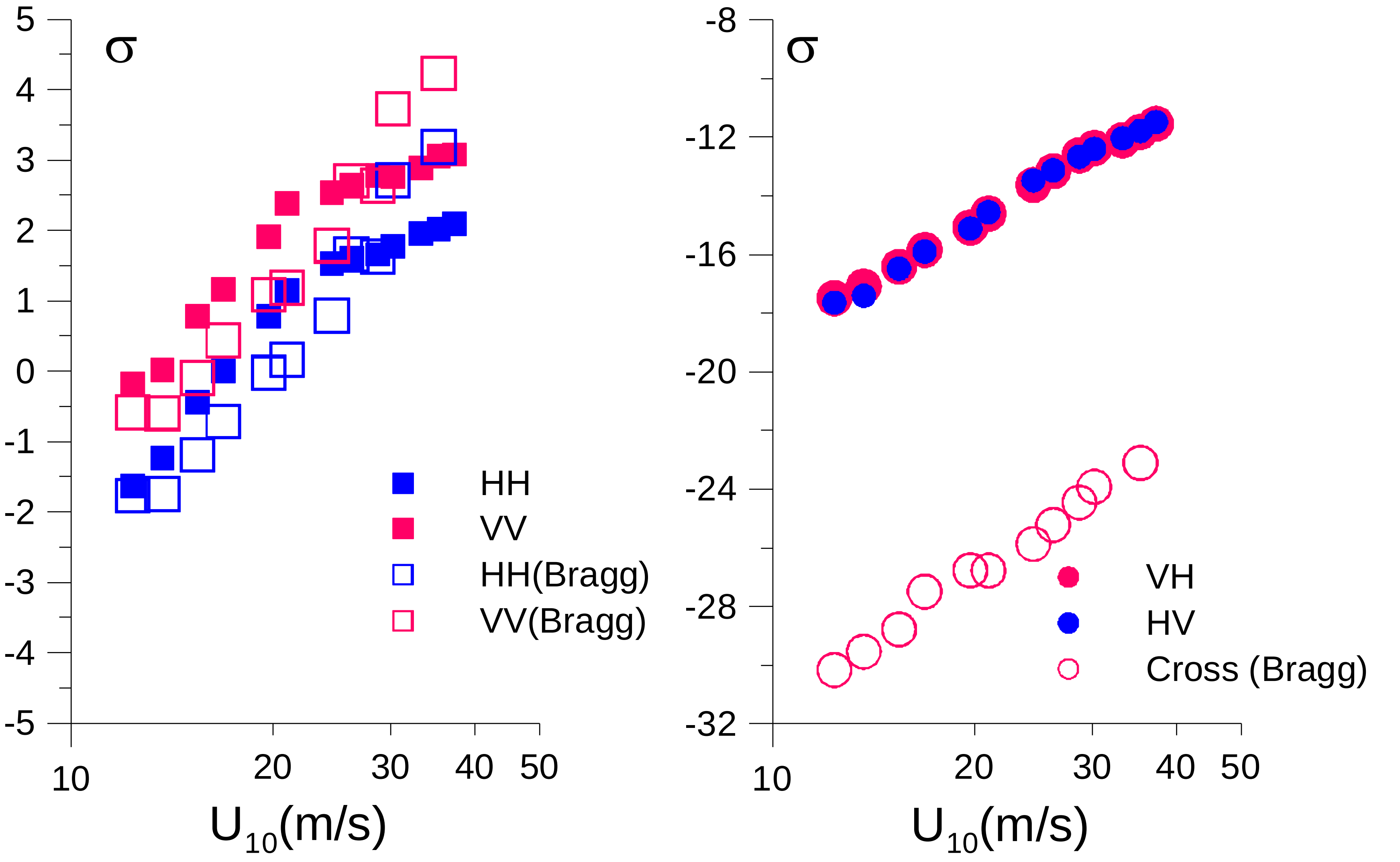

Doppler spectra of co-pol and de-pol X-band microwave return at different wind speeds at an incidence angle of 30º looking upwind plot via equivalent velocity of the Bragg scatters:

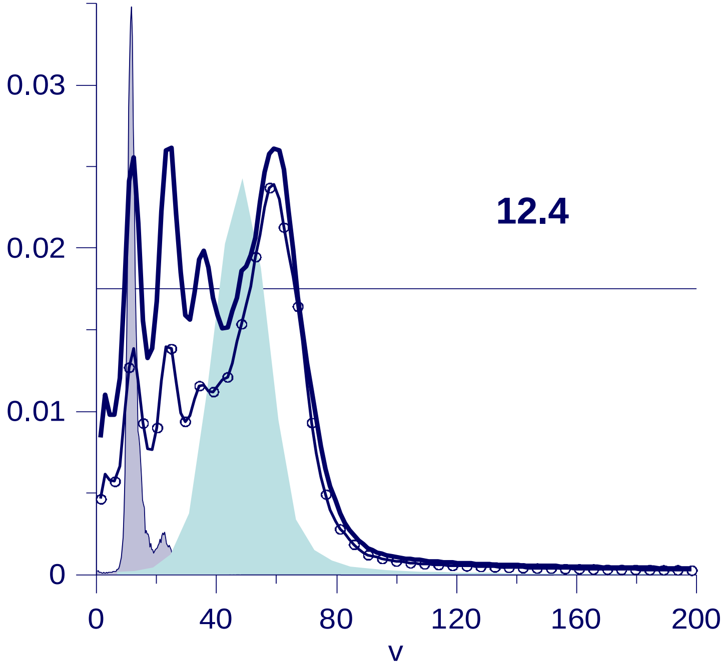

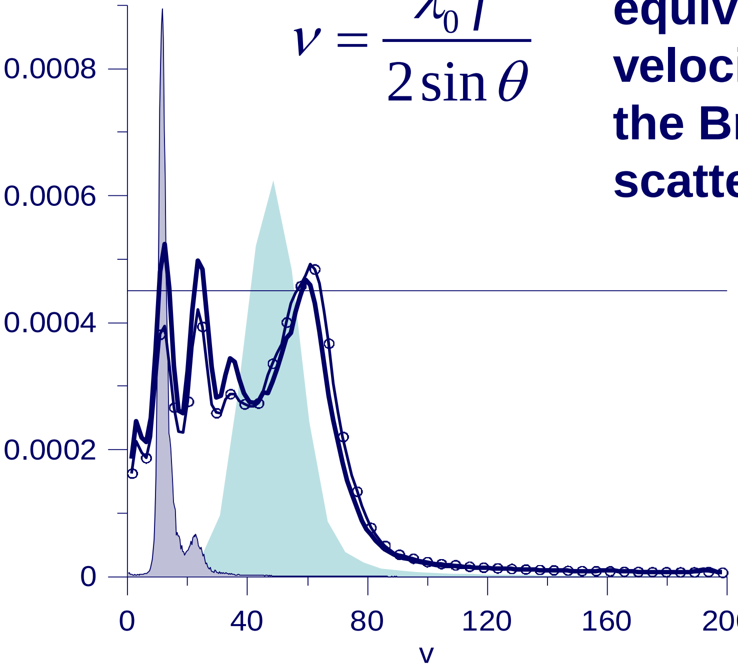

$$v = \frac{\lambda_0 f}{2\sin\theta}$$

equivalent velocity of the Bragg scatters

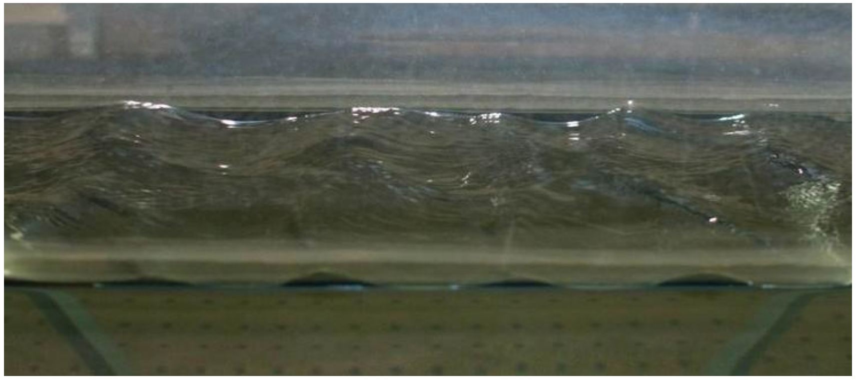

Side view of the water surface for 10-m wind speed 12.4 m/s

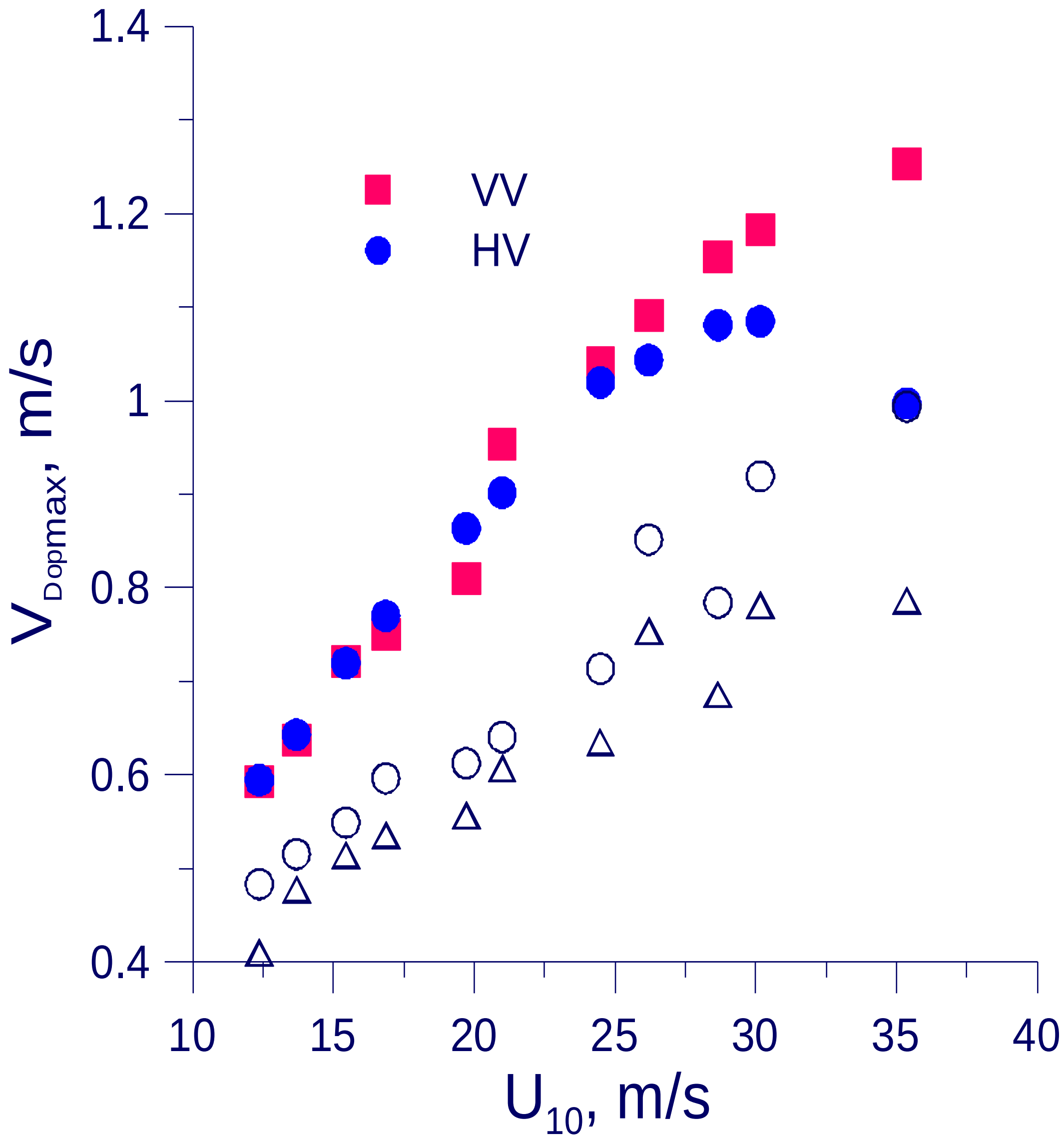

Max of the Doppler spectra of co-polarized and de-polarized radar return and and Max in the wind wave spectra via 10-m wind speed: open circles – for the complete spectra, open triangles – for the short wave part

Mechanism of droplet formation under strong wind over sea (U_{10}=25 m/s) Taken at 4500 fps, reproduced at 25 fps

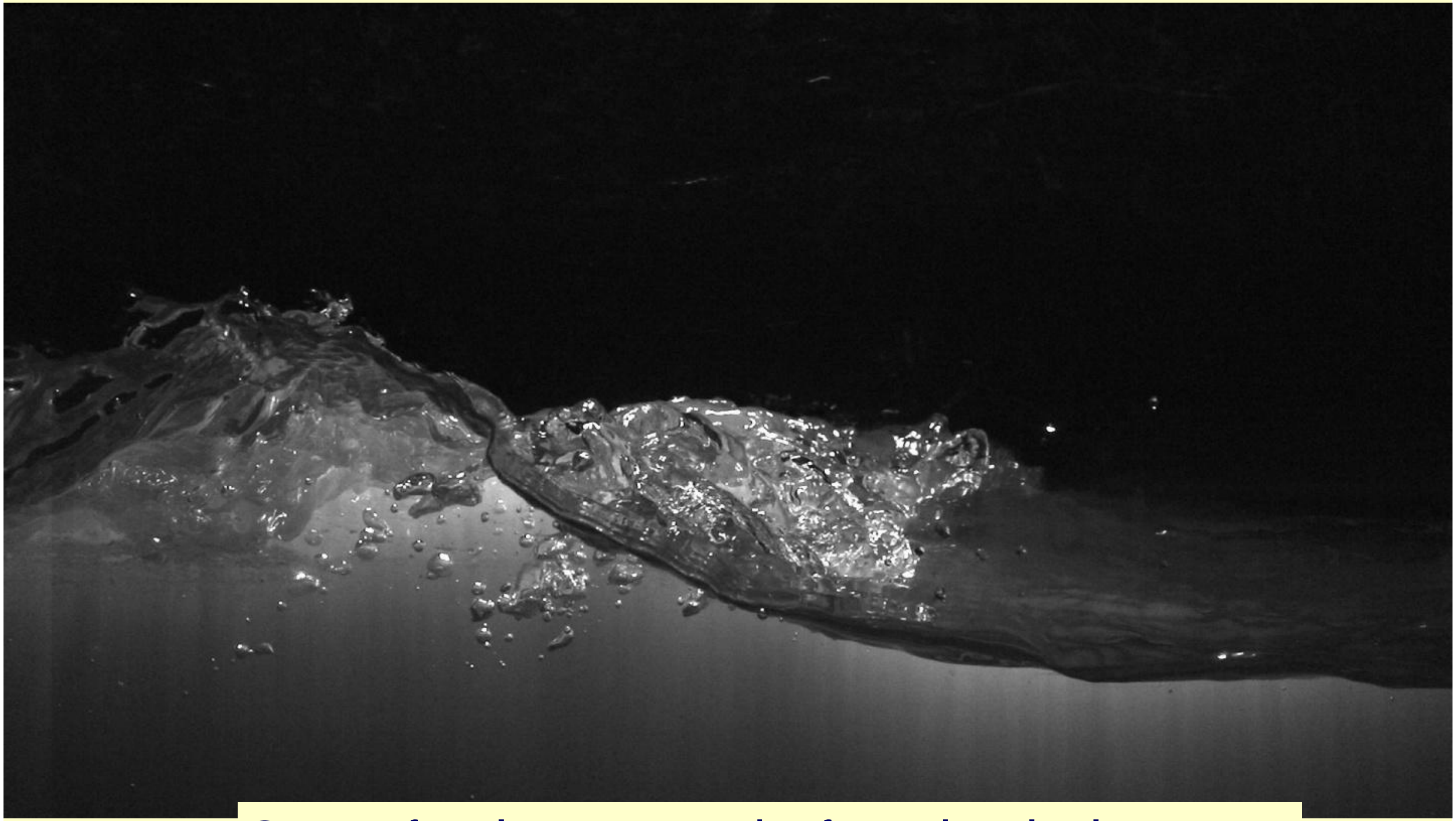

Scatters for microwaves moving faster than dominant wave:

•**small-scale structure of the wave-breaker**

•**bubbles inflating by wind and bursting to form droplets**

Mean σ_{0VH} from RADARSAT-2 dual-polarization SAR vs in situ–measured U_{10} from buoys, SFMR data, and H*Wind from B. Zhang et al., J. Atmos. Ocean. Tech., vol. 31, no. 2, pp. 272–286, Feb. 2014 and superimposed laboratory data-7.9dB (magenta points)

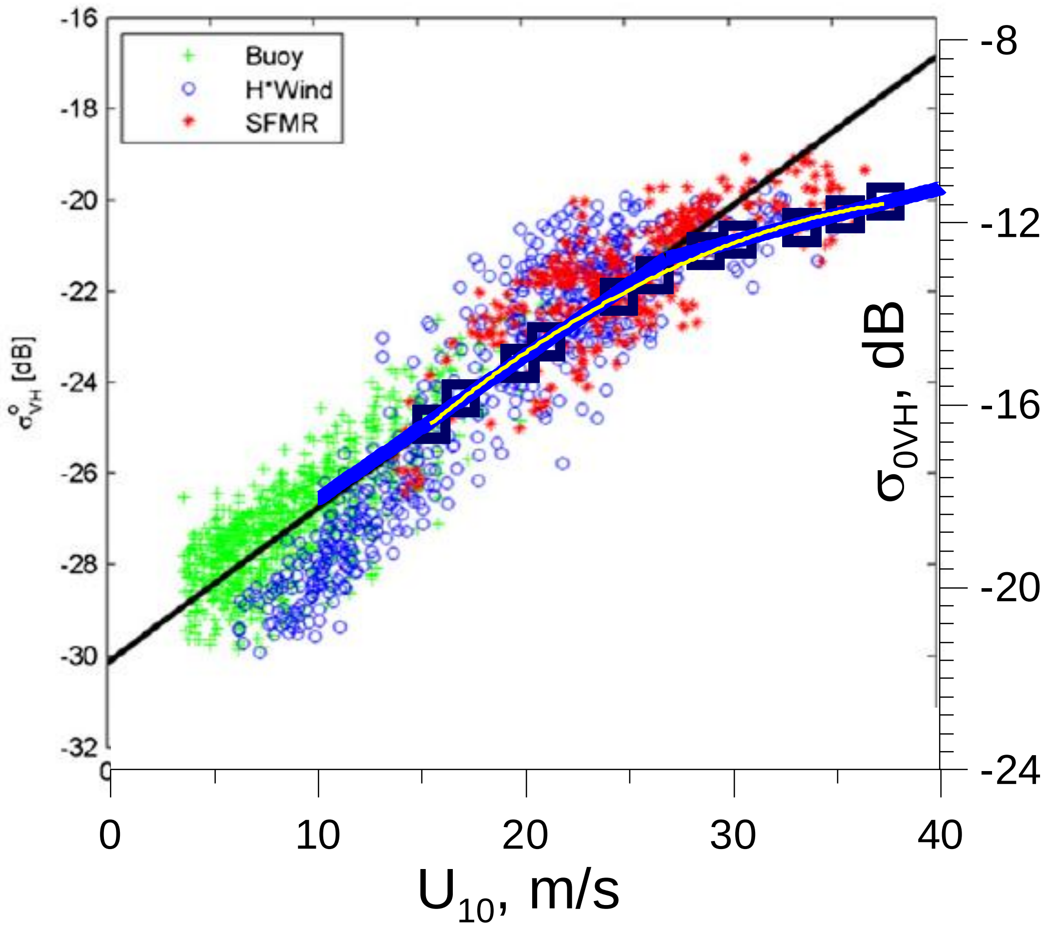

Difference in X and C NRSC

$\sigma_{0VHC}-\sigma_{0VHX}=-7.9$ dB

GMF for X -band

$\sigma_{0VH} = -21.2 + 0.314U_{10}$

for $U_{10}<26.8$ m/s

$\sigma_{0VH} = -17.2+0.153U_{10}$

for $U_{10}>26.8$ m/s

GMF for C –band (bi-linear)

$\sigma_{0VH} = -29.1 + 0.314U_{10}$

for $U_{10}<26.8$ m/s

$\sigma_{0VH} = -25.1+0.153U_{10}$

for $U_{10}>26.8$ m/s

GMF for C –band (polynomial)

$\sigma_{0VH} = -32.3 + 0.637\, U_{10} - 0.0077\, U_{10}^2$

Comparing wind speeds in the hurricane Earl at 2259 UT C 2 Sep 2010 retrieved by C-2PO algorithm (blue open circles B.Zhang, W.Perrie . BAMS, April 2012) and the new de-pol algorithm (red circles)

$$\sigma_{0VH} = -32.3 + 0.637\ U_{10} - 0.0077\ U_{10}^{2}$$

$$\sigma_{0VH} = =0.580 U_{10} - 38.7$$

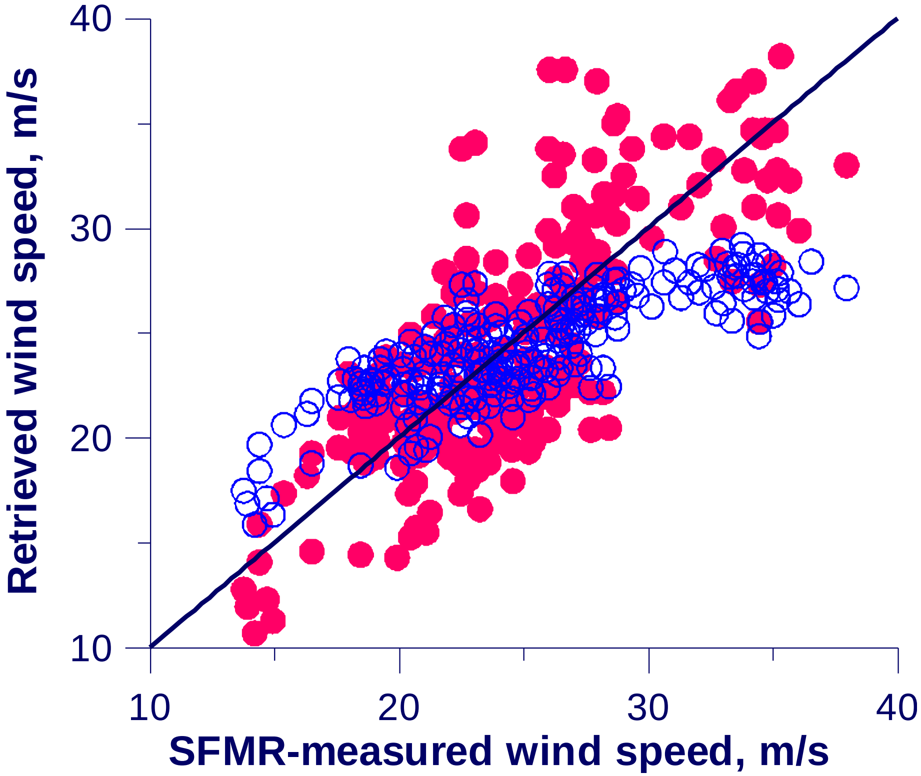

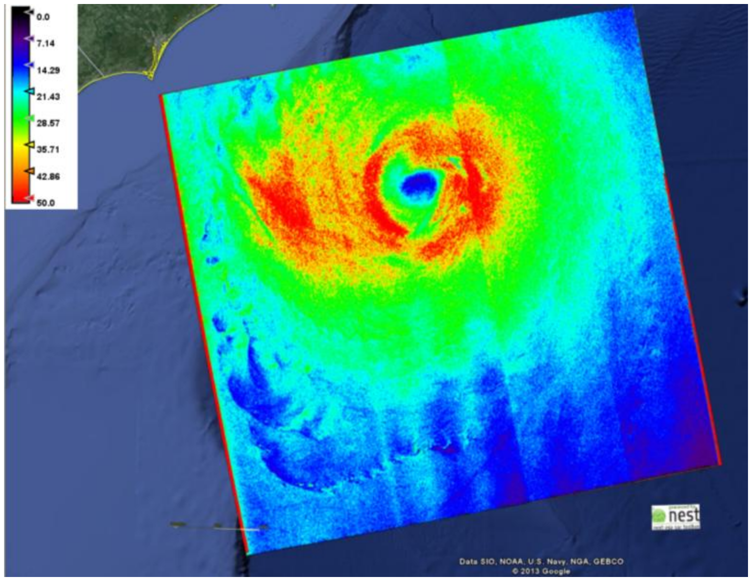

http://atmoc.iapras.ru/

Conclucions

- Complex structure of a tropical cyclone can be clearly seen from SAT images
- There are strong principal problems of hurricane winds retrieval from scatterometry due to the saturation of dependency of radar cross-section of the water on wind speed
- A solution is using de-polarized return from the water surface, which does not saturate at strong winds.
- The tendency to saturation still exists for high winds, but the sensitivity to wind speed is conserved up to 40 m/s.
- No enough statistics for winds over 40 m/s. Hope for lab data.
- A realistic theory of depolarized radar is required.

Thank you for your attentlon